# Synthesis and characterization of phosphonic acid functionalized maleic anhydride co-polymer for recovering scandium: Acidic red mud leachate as a case study

Mohammed Hamza, Hamed Mira, Shunyan Ning, Xiangbiao Yin, Ji Wang, Yuezhou Wei, Eric Guibal

# Synthesis and characterization of phosphonic acid functionalized maleic anhydride co-polymer for recovering scandium: Acidic red mud leachate as a case study

Mohammed F. Hamza [a,b,*], Hamed Mira [b], Shunyan Ning [a], Xiangbiao Yin [a], Ji Wang [a,*], Yuezhou Wei [a,c], Eric Guibal [d]

[a] School of Nuclear Science and Technology, University of South China, Heng Yang 421001, China
[b] Nuclear Materials Authority, POB 530, El-Maadi, Cairo, Egypt
[c] School of Nuclear Science and Engineering, Shanghai Jiao Tong University, Shanghai, China
[d] Polymers Composites and Hybrids (PCH), IMT Mines Ales, Ales, France

*Keywords:*
Bifunctional sorbent for efficient endothermic removal of scandium
Metal sorption is described by the Langmuir equation (isotherm) and the pseudo-first order rate equation (kinetics)
Easy metal desorption and stable sorbent recycling
Preference for scandium over light REEs > trivalent transition metal ions > divalent metal ions
Treatment of acidic leachate of red mud

## HIGHLIGHTS

- Scandium sorption strongly sorbed by carboxylate and phosphonate groups at pH 4.
- Endothermic sorption with capacity increasing up to 6.5 mmol Sc $g^{-1}$ at T: 50 °C.
- Fast kinetics (15–30 min), kinetics fitted by pseudo-first order rate equation.
- Metal desorption using 0.3 M HCl solu-tion (remarkable stability at fifth cycle).
- Sorption selectivity: Sc(III) > Light REEs > Trivalent cations > divalent cations.

## GRAPHICAL ABSTRACT

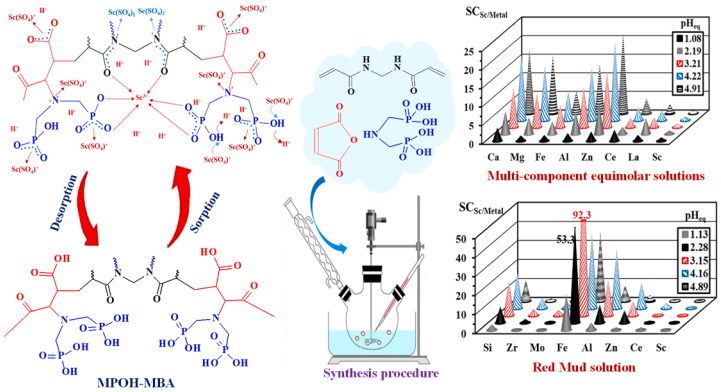


## ABSTRACT

A simple one-pot reaction of maleic anhydride with iminodi(methylphosphonic acid) in presence of N,N'- methylenebisacrylamide allows producing a micron-sized multifunctional sorbent (herein called MPOH-MBA, bearing both carboxylate, phosphonate groups, and tertiary amine groups). These multifunctional groups bring high reactivity for rare earth elements (REEs, hard acids) (soft bases O-bearing ligands, consistently with Pearson's principle) with modulation of positively-charged surface (amine groups for interaction with scandium sulfate species). Effectively, MPOH-MBA shows remarkable sorption capacity for Sc(III) at optimum initial pH (i. e., $pH_0$: 4): $q_{eq,exp}$ reaches up to 5.34 mmol Sc $g^{-1}$, at room temperature. Langmuir equation fits well experi-mental profiles (affinity coefficient: 0.677 L $mmol^{-1}$). Scandium sorption is endothermic: sorption capacity in-creases up to 6.50 mmol Sc $g^{-1}$ (at T: 50 °C), while the affinity coefficient increases up to 1.54 L $mmol^{-1}$. Fast kinetics (equilibrium reached in 20–30 min) are favored by the micron-size of the sorbent (and its good textural properties: 51 m2 g 1 for specific surface area and pore width close to 250 Å). Kinetic profiles are fitted by the pseudo-first order rate equation. The sorbent can be easily regenerated using 0.3 M HCl solution; the loss in sorption is less than 1.5% at the fifth cycle. Main reactive groups (identified by Fourier-transform infrared spectroscopy) are carboxylate and phosphonate groups. In presence of equimolar concentrations of competitor ions: sorption is governed by preference for trivalent metal ions over divalent cations. Among trivalent metal ions rare earth elements (REEs) are preferentially bound (against Al(III) and Fe(III)); in addition, MPOH-MBA sorbs Sc (III) with higher affinity than Nd(III) and Ce(III). The sorbent shows a relative selectivity for scandium and REEs over metal ions present in huge excess (100–500 excess), such as Fe(III) and Al(III)), in red mud acidic leachate.

* Corresponding author at: School of Nuclear Science and Technology, University of South China, Heng Yang 421001, China.
*E-mail addresses:* m_fouda21@usc.edu.cn (M.F. Hamza), wangji@usc.edu.cn (J. Wang).

## 1. Introduction

Though scandium is not formally included in the list of rare earth elements (REEs), its chemical properties (and presence in usual REE ores) made it being associated to critical metals (and included in the US Department of Commerce: 35 Critical Metals List in 2018, updated in 2022, [1]). Abundant but dispersed in ores [2,3], scandium is commercially recovered as a byproduct of the extraction of other valuable metals [4] from diverse sources, such as red mud [5–10], electronic scraps [11], tungsten slags [12], phosphogypsum, and uranium leachate [13]. Scandium is mainly used in the manufacturing of aluminum alloys (for enhanced resistance to mechanical constraints and corrosion), solid oxide fuel cells, electrical conductors, 3D printing (for aluminum-based components), and lithium-ion batteries.

Brouziotis et al. [14] analyzed the bibliography relative to the health and diseases associated with exposure to REEs (through occupational activities and food chain intake); they reported a series of diseases involving cytotoxicity (due to reactive oxygen species and DNA (deoxyribonucleic acid) damage), up to cell death. Ghosh et al. [15] reported the environmental impact along the production chain (for different Sc sources) at extraction, leaching, solvent extraction, sorption, and purification steps (including recycling from wastes). Based on these strategic, health, and environmental constraints, an increasing attention has been directed in the last decade to the development of new methods and materials for the recovery of scandium [9] and its separation from associated metals and REEs [16,17]. Frequently, the first step in these processes consists in the leaching of the metal from solid phases (mineral, waste, residues, red mud, etc.) [18–20]. The treatment of leachates or acid mine drainage may involve different techniques such as selective precipitation [21,22], solvent extraction [23–26], biosorption [27] or sorption [28–30]. Most of solvent extraction systems involve organophosphorus moieties [19,31,32], alkyl phosphinic acids [31,33], phosphonic acid [31], aminophosphonic group [34], and binary extractants (containing phosphonate-based and alkyl carboxylic acid compounds) [35]. Many sorbents have been designed for the recovery of scandium, including biosorbents [36,37], bio-based materials [38–40], resins [41–45], functionalized silica [46–51], and carbon nanotubes [52–54]. At the interface between solvent extraction and sorption techniques, solvent impregnated resins (or silica support) offer complementary opportunities [35,55,56], making more specifically profit of phosphonate-based extractants [57].

The strong affinity of phosphonate groups for this kind of metal ions (including REEs) may explain the interest attached to the use of iminodi (methylphosphonic acid) (IDMPA) as a ligand for such metal ions [58–61]. This property was used for elaborating photoluminescent materials (with rare earth elements: [62,63]), contrasting agent in nuclear magnetic resonance (with lanthanum, [64]), electrocatalysts (including application to water splitting, [65–67]), or manufacturing batteries [68]. This was also used for elaborating sorbents by grafting onto chitosan for the recovery of In(III), Sn(II), Th(IV), and U(VI) [60], and the functionalization of alginate-PEI beads (for the removal of Sr(II) and Cs(I)) [69].

On the other side, maleic anhydride (MAn) was used as a precursor for designing many resins through reaction with different functional polymers or precursors [70–73]: amine groups [74], thiourea [71], sulfonated groups [75], and peptide groups [76].

Based on the properties of MAn and IDMPA, a new sorbent was designed (MPOH-MBA) using N,N'-methylenebisacrylamide (MBA) as the crosslinker. The sorbent bears both carboxylic groups (from MAn) and phosphonate groups (from IDMPA), in addition to tertiary amine groups. It is noteworthy that the steric hindrance around tertiary amine groups in MPOH-MBA may control the accessibility of reactive groups. This system mimics the impregnated resin designed by Sharaf et al. [35] for the selective recovery of scandium: Amberlite XAD-7HP resin was associated with a mixture of two extractants: PC-88A (alkyl phosphonate) and Versatic 10 (based on carboxylic groups). The immobilization of functional groups on the organic backbone is expected to produce a stable solid sorbent (with reduced loss of extractant). The rational for designing this sorbent is based on the readily reaction of MAn with MBA (for structuring the resin) but also with IDMPA. The grafting of O-bearing ligands brings highly reactive and selective groups for the binding of REEs (according the Hard and Soft Acid and Base principles: hard bases react preferentially with hard acids). In addition, the presence of tertiary amine brings positively-charged reactive groups in acidic solutions (favorable for the sorption of anionic scandium sulfate species through anion exchange mechanism).

The multifunctional resin is initially characterized (by textural analysis, scanning electron microscopy, thermogravimetric analysis, Fourier-transform infrared spectrometry (FTIR), $pH_{PZC}$ (point of zero charge), and elemental analysis), before extensively investigating Sc(III) sorption properties. The effect of the pH is first considered (in relation with $pH_{PZC}$ and metal speciation). Uptake kinetics, sorption isotherms, and metal desorption (and sorbent recycling) are evaluated before investigating the selectivity from multicomponent equimolar solutions (with synthetic solutions, at different pH values). In the last part, the material is applied to Sc(III) recovery from real complex effluent (acidic leachate of red mud): the sorption capacities, distribution ratio, and selectivity are compared for Sc(III) (and other metal ions) to demonstrate the interest of MPOH-MBA for scandium recovery (and separation) from industrial effluent.

## 2. Materials and methods

### 2.1. Reagents

Iminodi(methylphosphonic acid) (IDMPA, 97%), maleic anhydride (MAn, 99%), 2-butanone (99%), N,N'-methylene bis-acrylamide (MBA, 99%), acetone (≥99.5%), potassium persulfate (KPS, ≥99%), and sodium hydroxide (≥ 97.0%) were supplied by Sigma-Aldrich (Merck KGa; Darmstadt, Germany). Scandium sulfate (99%), lanthanum sulfate (99%), and cerium sulfate (99%) were purchased from the National Engineering Research Center of Rare Earth Metallurgy and Functional Materials Co Ltd. (Baotou, China). Calcium chloride (99.1%), ferric sulfate (97.0%), magnesium chloride (95.0%), aluminum chloride (99.1%), and zinc chloride (98.0%) were obtained from Guangdong-Guanghua Sci. Tech., Co., Ltd., Guangdong, China.

### 2.2. Synthesis of sorbent

The sorbent was synthesized by the one-pot free radical

polymerization of maleic anhydride (MAn) with iminodi(methylphosphonic acid) (IDMPA) in polar aprotic solvent using potassium persulfate (KPS) as the redox initiator and N,N'-methylenebis(acrylamide) (MBA) as the crosslinking agent (Scheme 1) [77,78]. Practically, MAn (2.94 g, 30 mmol) and IDMPA (6.15 g, 30 mmol) were mixed in anhydrous 2-butanone (50 mL). Then, MBA (2.31 g, 15 mmol) was added to the mixture and vigorously mixed to produce a homogenous dispersion, before adding KPS (0.3 g), under reflux, at 80–85 °C. After successive washing steps using acetone and water, the white yellowish precipitate (MPOH-MBA) was dried at 60 °C overnight. The amount of produced sorbent reached 10.15 g; meaning that the conversion yield is close to 89% (based on weight balance).

### 2.3. Characterization of materials

Fourier-transform infra-red spectra were collected using an IR Tracer-100 FTIR spectrometer (Shimadzu, Tokyo, Japan). The samples were grinded with KBr powder and pressed into a disc (KBr pellet). The morphology of the materials was assessed using a Phenom ProX scanning electron microscope (equipped with an energy disperse X ray diffraction detector, Thermo-Fisher Scientific Eindhoven, Netherlands). Samples were carbon-coated, and the applied voltage was set to 15 kV. Elemental analysis was determined using a Vario EL-cube element analyzer (Elementar Analysensysteme GmbH, Langenselbold, Germany). The textural properties were characterized by $N_2$ adsorption and desorption isotherms using TriStar (II) analyzer (Micromeritics, Norcross (GA), USA); the sorbent samples were swept in $N_2$ atmosphere for 4 h at 120 °C, before analysis. The specific surface area ($S_{BET}$; $m^2\ g^{-1}$) was calculated using BET equation (Brunauer-Emmet-Teller isotherm), while the BJH method (Barret-Joyner-Halenda model) was used for evaluating the pore size and porous volume. The pH of zero charge was measured by the pH-drift method [79]. Sorbent samples (sorbent dose, SD: 2 g $L^{-1}$) were dropped in a series of flasks containing pH-adjusted solutions of 0.1 M NaCl (initial pH, $pH_0$, from 1 to 11). After contact for 48 h, under agitation, the final pH ($pH_{eq}$) was measured using a S220 seven-Compact pH ionometer (Mettler Toledo, Instruments; Shanghai, China). The $pH_{PZC}$ was defined as the pH value that corresponds to $pH_0$=$pH_{eq}$. The thermal degradation of the sorbent was analyzed under nitrogen atmosphere using a STA 449 *F3* Jupiter® thermoanalyzer (Netzsch-Gerätebau HGmbh, Selb, Germany), adopting a temperature ramp of 10 °C $min^{-1}$.

### 2.4. Sorption studies

The first part of the study was performed on synthetic solutions using the batch method. A given amount of sorbent (m, g) was mixed (at stirring velocity: 210 rpm) with a fixed volume of solution (V, L) containing Sc(III) (and other metal ions, when relevant) at $C_0$ initial concentration (mmol Sc $L^{-1}$) and given $pH_0$. After fixed contact times (for uptake kinetics, or 48 h for most equilibrium experiments), samples were collected, and filtrated (filter membrane, pore size ≈1.2 μm); the equilibrium pH and the residual concentration (at equilibrium $C_{eq}$, or at time t; C(t), mmol Sc $L^{-1}$) were measured. Metal concentrations were analyzed by inductively coupled plasma atomic emission spectrometer (ICPS-7510, Shimadzu, Tokyo, Japan). The distribution ratio (D, L $g^{-1}$) was calculated from: $D = q_{eq}/C_{eq}$. The mass balance equation was used for the determination of sorption capacity (at equilibrium, $q_{eq}$, or at time t, q(t), mmol Sc $g^{-1}$): $q_{eq} = (C_0\text{-}C_{eq}) \times V/m$. For multi-component solutions (selectivity study), the same experimental procedure was adopted using equimolar concentrations of selected metal (or metalloid) ions. The selectivity coefficient ($SC_{Sc/metal}$) was defined by:

$$SC_{Sc/metal} = \frac{D_{Sc}}{D_{metal}} = \frac{q_{eq,Sc} \times C_{eq,metal}}{C_{eq,Sc} \times q_{eq,metal}} \quad (1)$$

For the study of metal desorption, the samples collected from uptake kinetics (with known sorption capacity) were mixed with a fixed volume of eluent (i.e., 0.3 M HCl); the sorbent dose (SD) was fixed to 2 g $L^{-1}$ (SD = 0.667 g $L^{-1}$ for sorption step). For recycling tests, a water washing step was systematically intercalated between each sorption and desorption steps. Mass balance equations were used for calculating sorption and desorption efficiencies and comparing the relevant performances with those obtained at the first step.

The experiments were duplicated, and the data are reported as the average values with standard deviation. The experimental conditions are systematically recorded in the caption of the figures.

Conventional models were used for fitting experimental curves for uptake kinetics and sorption isotherms; these equations are summarized in Table S1 (see Supplementary Information). The parameters were determined using non-linear regression analysis (with Mathematica® facilities, Wolfram Research, Champaign, IL, USA). The quality of the fits was assessed using the determination coefficient (i.e., $R^2$) and the Akaike Information Criterion (AIC, [80]).

### 2.5. Application to industrial effluent

The testing of MPOH-MBA with real industrial effluent was performed on bauxite residues (red mud) generated by Jinnao-Ti Co (Tengixan, Guangxi, China). The red mud was washed up with water before being leached with sulfuric acid in the company. The produced acidic leachate was used for these sorption tests. The effluent contains a wide diversity of metal ions, (i.e., alkali, alkali-earth, transition and non-transition elements, mainly Al and Fe, but also Si, Zr, Ti, Zn, Mo, and REEs). The (as-produced) highly acidic solution (pH below zero) was firstly adjusted to 1 (using 0.1/1 M NaOH solutions). The composition of the solution for target elements (see above) in this solution (as reference) is reported in Table S2. Sorption tests were performed at different pH values (in the range $pH_0$: 1–5, using NaOH solutions); Table S2 summarizes the loss of target metals during pH adjustment (some alternative data such as effective metal concentrations and molar excess compared with scandium are also compiled). The contact time was set at 24 h, and the SD value to 1 g $L^{-1}$. After sorption, the equilibrium pH was measured before filtration, the residual concentrations were determined

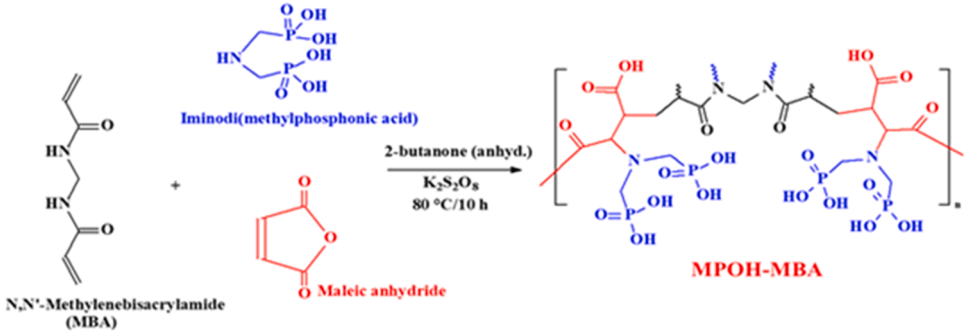


**Scheme 1.** Synthesis procedure for the preparation of MPOH-MBA.

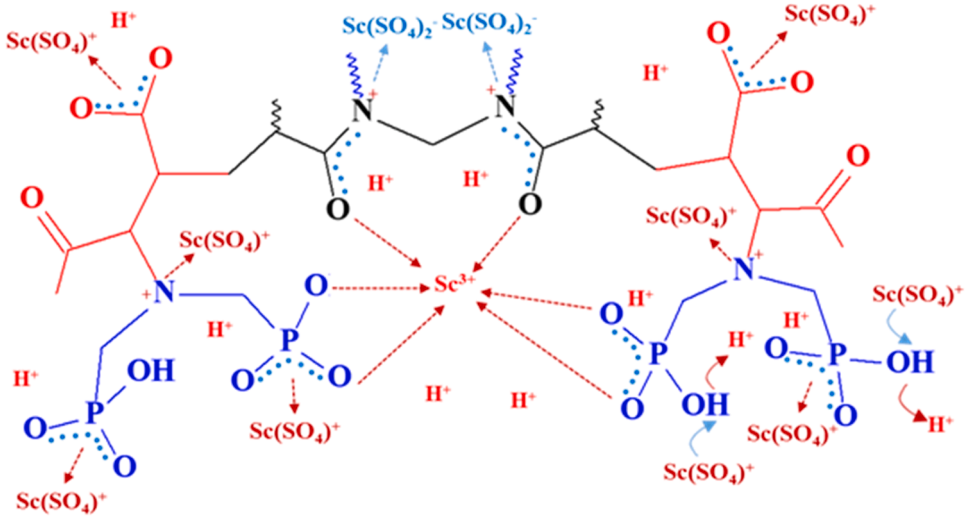


**Scheme 2.** Suggested mechanisms for Sc(III) binding onto MPOH-MBA.

by ICP-AES for calculating sorption capacity, concentration factor (X-factor: $q_{eq}/C_0$), distribution ratio (i.e., D), and $SC_{Sc/metal}$.

## 3. Results and discussion

### 3.1. Characterization of sorbent

#### 3.1.1. Physical properties

Scanning electron microscopy shows that sorbent particles obey a heterogeneous distribution in terms of both shape and size (3–15 μm, average ≈7.5 μm) (Figure S1). Particles are roughly spherical, with granular surfaces and/or layered structure (platelet-like stacks). Nitrogen adsorption-desorption isotherms are reported in Figure S2a. In the IUPAC classification (International Union of Pure and Applied Chemistry), this isotherm is assimilated to a Type II curve. This type of isotherm corresponds to the adsorption of gas on nonporous or macroporous materials. This could be also assigned to Type IV isotherm (with limited saturation plateau (pore condensation zone). In this case, the material is supposed to be mesoporous. The two branches (adsorption *vs.* desorption) are separated; the hysteresis loop is typical of Type IVa classification, which corresponds to mesoporous structure (with pore width larger than 4 nm) [81]. The hysteresis loop may be classified as H2b (with the absence of the saturation plateau) or H3 (with the absence of the cavitation point). The BET equation was used for the determination of the specific surface area of the sorbent, which is close to 51 $m^2\ g^{-1}$. The BJH equation was applied to both adsorption and desorption branches: porous volumes are close to 0.219 and 0.229 $cm^3\ g^{-1}$, respectively. In Figure S2b, the distribution of pore widths is almost Gaussian centered around 250 Å. This is larger than the pore size deduced from BJH equation: 170 Å (adsorption branch) and 143 Å (desorption branch). According to IUPAC classification of pores, MPOH-MBA can be considered mesoporous (20 Å < mesoporous <500 Å).

The study of thermal degradation (Thermal Gravimetric Analysis, TGA) under nitrogen atmosphere shows three major transitions (Figure S3):

(a) < 195.1 °C: weight loss (WL) reaches ≈17.6%, corresponding to the release of adsorbed water from the sorbent; the peak on the DTG profile (differential thermogravimetric) is attained at 56.9°C,
(b) 195.1–400.5 °C: WL = ≈43.1%; the DTG is marked by two peaks at 249.3 °C and 387.7 °C. At this stage, the material depolymerizes, carboxylate and phosphonate groups may be decomposed. Afonin [59] reported the degradation of iminodimethylphosphonic acid above 245 °C by pyrolysis of P-C bonds.
(c) 400.5–803.5 °C: WL = 30.8%; two small DTG peaks are detected at 572.8 °C and 644.7 °C. The final degradation of phosphonate occurs in this region together with the degradation of the char. The total weight loss reaches 91.5%.

In the case of TGA analysis of (carboxymethyl) iminodi(methylphosphonic acid) complexes with Nd(III) and Eu(III), Cunha-Silva et al. [63] identified three steps: at 115–125 °C (WL: 1.8–3.0%), 250–390 °C (WL: 10–11%), and 390–700 °C (WL: 4–6%).

#### 3.1.2. Chemical properties

Fig. 1 and Figure S4 show the FTIR spectra of the sorbent at different stages of use (raw, after conditioning at pH 4, after Sc(III) sorption at pH 4, and after five cycles of sorption and desorption). In the wavenumber range 4000–2000 $cm^{-1}$ (Figure S4), a broad band is identified at 3424 ±2 $cm^{-1}$, which is associated to the convolution of the $\nu_{N\text{-}H}$ and $\nu_{O\text{-}H}$ signals. Herein, the amine group is present as tertiary amine (Scheme 1) and most of the band should be assigned to the numerous OH groups hold by phosphonate moieties. Cunha-Silva et al. [63] investigated the complexation of Nd(III) and Eu(III) using (carboxymethyl) iminodi (methylphosphonic acid). They identified $\nu_{O\text{-}H}$ (in phosphonate) at 3583–3563 $cm^{-1}$, and $\nu_{O\text{-}H}$ (in water) at 3390–3405 $cm^{-1}$, while $\nu_{N\text{-}H}$ signal was associated with 3115–3120 $cm^{-1}$ band. It is noteworthy that after recycling the sorbent for 5 cycles, the broad band is restored, while for pH-4 conditioned material the weak shoulder at ≈3200 $cm^{-1}$ is weakened (as well as for Sc(III)-loaded sorbent). In addition, in the case of metal-bound sorbent, the peak is shifted toward higher wavenumber (i.e., 3453 $cm^{-1}$). It probably means that the chemical environment of –OH groups (in phosphonate moieties) is affected by Sc(III) chelation. In the region 1960–1850 $cm^{-1}$, the bands correspond to $\nu_{C\text{-}H}$ vibrations (in $-CH_2$, and $-CH_3$ groups). These bands are hardly affected by the experimental conditions (the resolution of the bands decreases after metal sorption). Another band is observed at 2378 $cm^{-1}$, which may be assigned to $\nu_{O\text{-}H}$ in phosphonate environment [82]; apparently, this band is not influenced by the modification of the sorbent (contrary to the shoulder on the broad band at 3200 $cm^{-1}$). More interesting are the comparisons of spectra appearing in Fig. 1 (for 1800–400 $cm^{-1}$ range). The band at 1740 (or 1734) $cm^{-1}$ is attributed to $\nu_{C=O}$ vibration in ketone and carboxylic groups [83] (MBA-MAn skeletal arrangement); this band is weakened after conditioning in pH 4 aqueous solution and disappears after scandium binding. The broad band appearing at 1647 $cm^{-1}$ is shifted to 1655 $cm^{-1}$ after adjusting the pH to 4 (and after

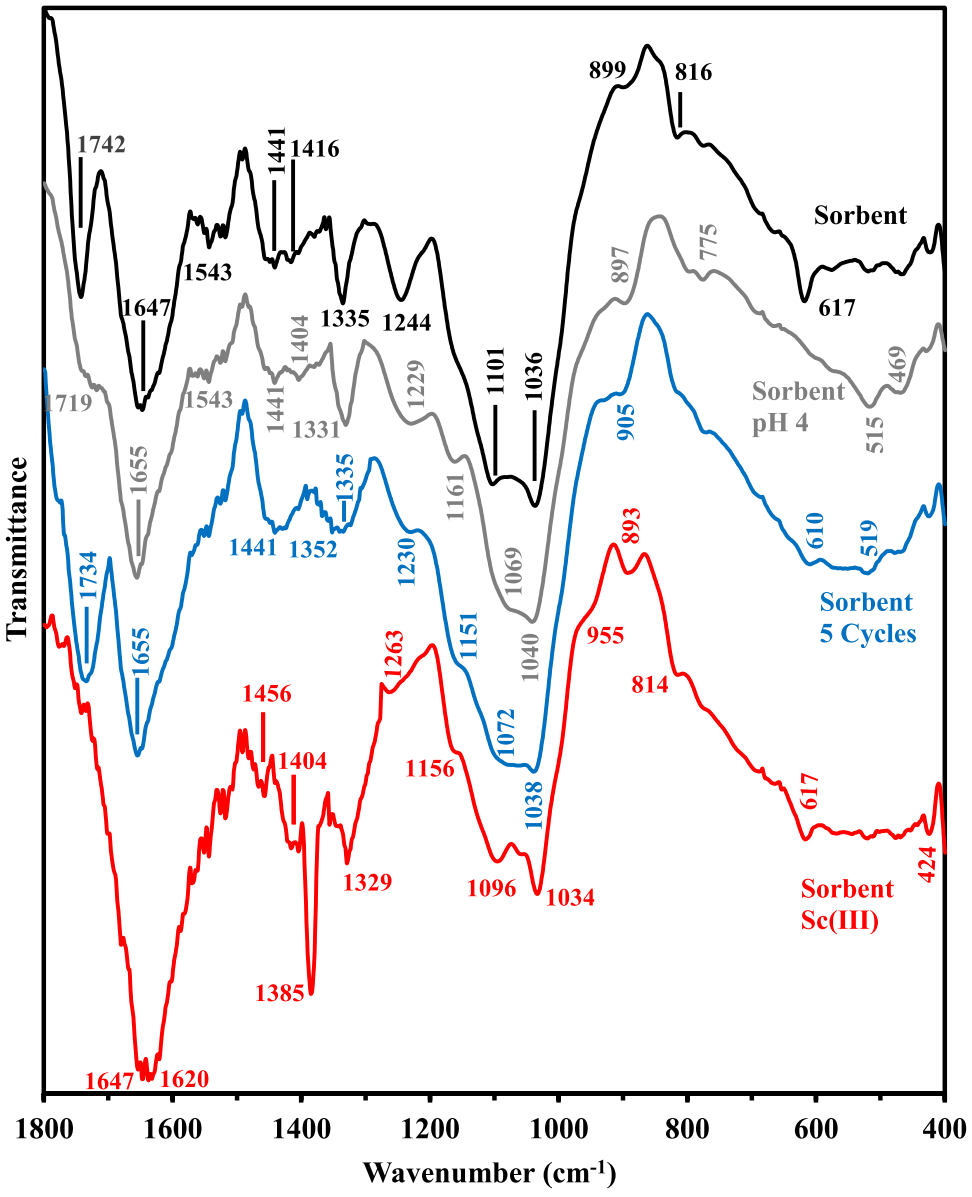


**Fig. 1.** FTIR spectra of MPOH-MBA sorbent at different stages of use: pristine sorbent, after conditioning at the pH of sorption (i.e., $pH_0$ 4), after Sc(III) sorption, and after 5 cycles of reuse (sorption/desorption) (wavenumber range: 1800–400 $cm^{-1}$).

five recycling steps), which is coupled to two bands observed at 1416–1404 $cm^{-1}$ and 1335–1331 $cm^{-1}$, which are assigned to asymmetric and symmetric $\nu_{COO^-}$ signals, respectively [63]. The broadness of the band is probably associated with the convolution of amine vibrations. Based on the value of $\Delta[\nu_{COO\text{-}asym} - \nu_{COO\text{-}sym}]$ (in the range 280–196 $cm^{-1}$), Cunha-Silva et al. [63] concluded that the binding of rare earths onto carboxylate moieties proceeds through the anti-unidentate coordination mechanism. Here, the Δ value ranges between 243 and 318 $cm^{-1}$; Deacon and Philips [84] correlated high Δ values with unidentate coordination of metal ions with acetate groups. After Sc(III) sorption, the band at 1647 $cm^{-1}$ is enlarged with a side contribution at 1620 $cm^{-1}$. It is noteworthy that a strong and sharp band appears at 1385 $cm^{-1}$ (which disappears after recycling). This results from the interaction of carboxylate groups with Sc(III) (with proton exchange) and/or formation of $N^+$ (following the binding of Sc(III), and relevant species) [85,86]. The band at 1335–1331 $cm^{-1}$, which is assigned to tertiary amine, is shifted to 1329 $cm^{-1}$ after scandium binding. The band at 1244–1229 $cm^{-1}$ is attributed to the overtone of in-plane $\delta_{P\text{-}OH}$ vibration, while the out-of-plane $\delta_{P\text{-}OH}$ vibration is found close to 897–905 $cm^{-1}$ [82]. After metal binding, the bands are shifted toward 1263 and 893 $cm^{-1}$, respectively. The $\nu_{P=O}$ vibration at 1036 $cm^{-1}$ shifts to 1040 $cm^{-1}$ at pH 4, while the sorption of Sc(III) causes the shift of the band back to 1034 $cm^{-1}$. Cunha-Silva et al. [63] identified the coordination of Nd(III) and Eu(III) with P-O moieties at 1157–1155 $cm^{-1}$ ($\nu_{P\text{-}Ocoord.,asym}$) and 1002–995 $cm^{-1}$ ($\nu_{P\text{-}Ocoord.,sym}$). Here, a shoulder appears after scandium binding at ≈955 $cm^{-1}$. The band corresponding to $\nu_{P\text{-}Ocoord.,asym}$ appears at 1156 $cm^{-1}$ for MPOH-MBA/Sc(III). This band is shifted from 1161 $cm^{-1}$ for protonated sorbent, while for pristine sorbent; the shoulder is hardly detectable (appearing at 1151 $cm^{-1}$ for recycled sorbent). The multiplicity of reactive groups offers different opportunities of interactions with Sc(III). The major contributions concern carboxylate and phosphonate groups, as indicated by the changes in FTIR spectra (amine groups are poorly active, by comparison). The recycling of the sorbent changes the FTIR spectrum of the sorbent, which is marked by (a) the weakening of the bands at 1244 and 1543 $cm^{-1}$, and (b) the widening of the band at 1335 $cm^{-1}$. However, the spectrum is roughly restored.

The $pH_{PZC}$ is found close to 4.8–4.9 (depending on the concentration

of the background salt, Figure S5). The strength and the density of acid groups (carboxylic and phosphonic groups) counter-balance the alkaline character of amine groups; this results in sorbent acidic behavior and positively-charged surface in acidic solutions. In the case of magnetic poly(glycidyl methacrylate) functionalized with iminodiphosphonate, Galhoum [87] found a $pH_{PZC}$ value close to 4.52.

The elemental analysis of the sorbent shows strong density of amine groups (N: 6.6%, 4.71 mmol N $g^{-1}$) and phosphonate moieties (P: 9.0%, 2.91 mmol P $g^{-1}$) (Table S3). Based on the structure of iminodiphosphonate (N:P = 1:2), nitrogen content assigned to IMDPA represents 1.45 mmol N $g^{-1}$; this means that 3.26 mmol N $g^{-1}$ come from MBA skeleton (1.633 mmol MBA). The yield of substitution reaches 44.5% on IMDPA. The twice excess of IMDPA compared with MBA means that the conversion reaches 89% (which is consistent with the weight balance between reagents and products). The incomplete conversion (in terms of mass balance) can be explained by the loss of precursors in the reactive phase. Szkudlarek et al. [76] investigated similar mode of reaction between maleic anhydride and 4-methyl-1-pentene (herein between MAn and MBA); the synthesis yielded 77%. They also reported that when the anhydride is added in excess, the reaction generally produces alternating copolymers. Teng et al. [88] synthesized a sorbent by the reaction of MAn with acrylamide (and MBA as a crosslinker). The Michael addition of amines to maleic anhydride has been described by Gurjar et al. [89]: the reaction of amine groups proceeds directly on the maleic anhydride cycle (on the fourth position). However, the reaction of maleic anhydride with acrylamide moieties of MBA limits the contribution of direct reaction of imino group with MAn.

### 3.2. Sorption properties

#### 3.2.1. Effect of pH

The pH critically influences the sorption properties through its intrinsic effects on the protonation/deprotonation of reactive groups ($pH_{PZC}$ value, Figure S5) and metal speciation (Figure S6, under the experimental conditions of the study of pH effect). Fig. 2 shows the effect of the pH on Sc(III) sorption at T: 21 ±1 °C and 50 ±1 °C, for low and high Sc(III) concentrations (i.e., 2.31 and 11.0 mmol Sc $L^{-1}$, respectively; Fig. 2). The two series show the same "parallel" curves; the increase in the temperature shifts the curves toward higher sorption capacities: overall, the Sc(III) removal by MPOH-MBA is endothermic. Obviously, increasing the concentration of Sc(III) increases metal sorption; however, the trends are consistent for the two systems. Indeed, at $pH_{eq}$ 1.14–1.21 sorption is "limited" ($q_{eq}$: varies between 0.37 and 0.58 mmol Sc $g^{-1}$). The sorption capacity increases almost linearly with the pH up to $pH_{eq}$ 4.16–4.30; while above this limit, $q_{eq}$ tends to stabilize; this is close to the value of $pH_{PZC}$ (i.e., 4.86 ±0.1). At $pH_{eq} \approx 4.9–5$, the sorption efficiency reaches 64% and 85% for $C_0$: 2.31 mmol Sc $L^{-1}$ at 21 °C and 50 °C, respectively (while achieves 33% and 38%, respectively, at $C_0$: 11.4 mmol Sc $L^{-1}$). With pH increase, the protonation of reactive groups continuously decreases (up to $pH_{PZC}$ value), which progressively limits the cationic repulsion effect. Indeed, most of scandium (>80%) is present under cationic sulfate form (i.e., $Sc(SO_4)^+$). Sorption proceeds essentially on phosphonate and carboxylate groups by chelation and proton exchange. The weak sorption observed at pH 1–2 may involve the binding of the anionic form (i.e., $Sc(SO_4)_2^-$, representing 13–8%), through anion exchange on protonated amine groups. The stabilization at pH superior to 4.5–5 may be explained by the complete deprotonation of reactive groups and by the progressive decrease of the concentration of absorbable species ($Sc(SO_4)^+$), which is replaced with hydrolyzed cations (i.e., $Sc(OH)^{2+}$, $Sc(OH)_2^+$ and the polynuclear form $Sc_2(OH)$

In Figure S7a, the distribution ratio (D, L $g^{-1}$) is plotted (as $\log_{10}$ plot) against equilibrium pH. The plot is almost linear between $pH_{eq}$ ≈1.1 and ≈4 with a slope that varies between 0.39 and 0.51 (depending on the system – i.e., $C_0$ and T), meaning that the sorption of one mole of sorbate is associated with the release of two moles of protons (assuming that ion-exchange mechanism is involved in Sc(III) binding). On the other hand, contrary to this hypothesis, the pH variation during sorption (appearing in Figure S7b) shows that the pH slightly increases (by less than 0.3 pH unit) up to ≈4.5, while above this limit value the equilibrium pH tends to decrease (by less than 0.2 pH unit). The boundary pH limit is again close to the $pH_C$ value. This contradictory trend probably means that the sorption process involves complex mechanism (based on contributions of ion-exchange/electrostatic attraction and chelation mechanisms). To prevent metal precipitation, which may occur at high metal concentration and at pH close to 5.7, further experiments are performed at pH 4.

The pH increases and the slope value for the $\log_{10}$ D plot against $pH_{eq}$

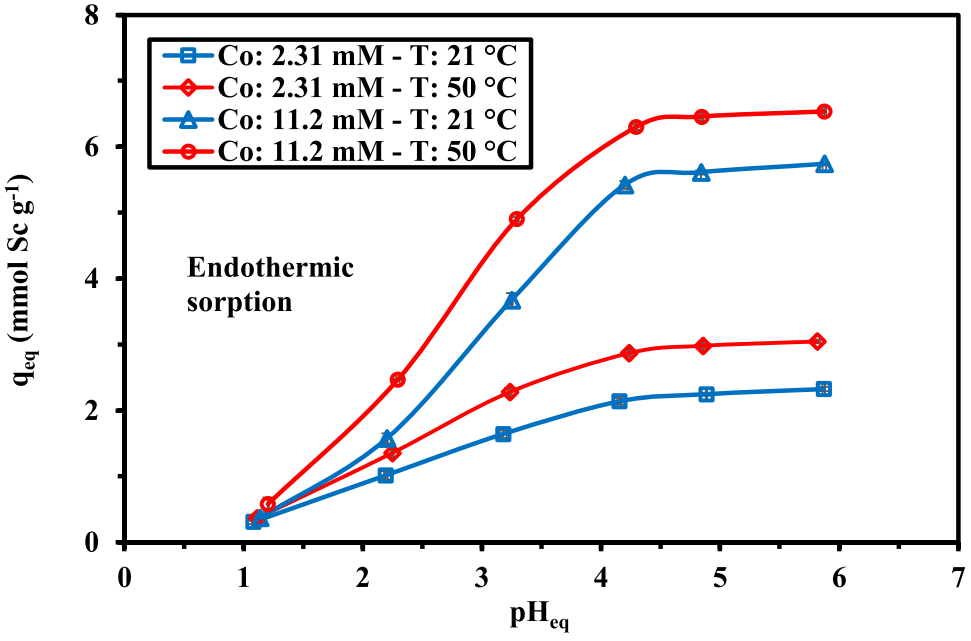


**Fig. 2.** Effect of pH on the sorption of Sc(III) using MPOH-MBA ($C_0$: 2.31 or 11.2 mmol Sc $L^{-1}$; T: 21 ±1 °C or 50 ±1 °C; Sorbent dose, SD: 0.67 g $L^{-1}$; time: 48 h; v- 210 rpm).

(closed to 0.4–0.5), may be explained by the release of 2 protons per Sc bound considering both ion-exchange (anion exchange at acidic pH) and chelation (cation binding at mild pH) mechanisms, through the conversion of tertiary amine to quaternary ammonium (identified by FTIR spectrometry).

In the case of Sc(III) sorption by ion-imprinted magnetic nanocomposite bentonite (bearing phosphonate groups, in chitosan/bentonite matrix), Wang et al. [90] reported a sigmoidal trend for the effect of the pH with negligible sorption below pH 3 and a maximum sorption at pH close to 5 (with stabilization above). In this case, the $pH_{PZC}$ was close to 2.5–2.7; scandium predominant forms were hydrolyzed species (under selected experimental conditions). Salman et al. [91] functionalized magnetic $SiO_2$ nanoparticles with either amine and carboxyl groups (as EDTA, ethylenediaminetetraacetic acid): they showed that Sc(III) form with EDTA moieties non-covalent interactions; consistently with Ramasamy et al. [47], they report the enhancement of metal complexation with pH increase (maximum at pH ≈5).

### 3.2.2. *Uptake kinetics*

Under selected experimental conditions ($pH_0$: 4; SD: 0.66 g $L^{-1}$, $C_0$: 2.28 and 11.0 mmol Sc $L^{-1}$, and at T: 21 °C and 50 °C), the equilibrium is reached within 20–30 min (Fig. 3). This may be easily explained by the small size of sorbent particles (i.e., ≈7.5 μm). The sorption occurs first at the surface of the sorbent and the diffusion pathway to reach the center of sorbent particles, which is short enough to promote fast sorption. This may be explained by favorable textural properties of MPOH-MBA (i.e., $S_{BET}$: 51 $m^2$ $g^{-1}$; pore size: 143–170 Å). It is noteworthy that the profiles are "parallel" for the two couples of kinetics: the temperature and the concentration logically affect the equilibrium concentration (and sorption capacity) but not the overall kinetic profiles. These kinetics are consistent with the profiles obtained with sulfonated alginate/PEI beads (though using here higher sorbent dose) [40]. Apparently, higher contact times are required for Sc(III) sorption onto functionalized magnetic $SiO_2$ sorbent [91]; however, different experimental conditions make complex the direct comparison of equilibrium times. Bao et al. [92] compared the kinetic profiles of a series of synthetic resins bearing aminomethyl-phosphonic acid (TP 260), iminodiacetic acid (TP 209), and bis-(2,4,4-trimethylpentyl)-phosphinic acid (TP 272) at pH 2.5. Despite lower Sc concentration and higher sorbent dose, the equilibrium times were much higher (i.e., 10–48 h); this is due to larger particle sizes (0.63 mm-1.6 mm) which may contribute to these slower profiles.

Sorption kinetics may be controlled by different mechanisms of resistance to diffusion (including bulk, film, and intraparticle diffusion), in addition to the proper reaction rate (which can be approached by PFORE and PSORE). Relevant models have been tested for fitting experimental profiles (Table S1a), Table 1 summarizes the parameters of the models (with statistical indicators). Both the values of determination coefficient (i.e., $R^2$) and Akaike Information Criterion (i.e., AIC) demonstrate that the best fits are obtained with the pseudo-first order rate equation (PFORE). In Fig. 3, the solid lines represent the fits of experimental profiles with the PFORE (using parameters reported in Table 1). The most difficult to simulate section is found in the region close to 15 min of contact, that corresponds to the higher curvature of kinetic curves. The fittings of experimental points by the PSORE and the RIDE (for resistance to intraparticle diffusion) are reported in Figure S8. This preference is corroborated by the values of calculated sorption capacities at equilibrium, which are closer to the experimental values: the PFORE overestimates experimental data by 2.4–4.2% (i.e., much lower than the discrepancies observed with PSORE: 14–20%). As expected, increasing the concentration (from 2.28 to 11.0 mmol Sc $L^{-1}$), enhances sorption capacity at equilibrium by 2.45 and 2.23 folds at T: 21 °C and 50 °C, respectively. As expected, temperature also promotes the equilibrium sorption capacity (+33% and +21% at $C_0$: 2.31 and 11.0 mmol Sc $L^{-1}$, respectively). The apparent rate coefficient (i.e., $k_1$) varies with experimental conditions in a limited interval: from 6.40 to 9.55 × $10^{-2}$ $min^{-1}$. Both metal concentration and temperature slightly increase $k_1$ values (by less than 1.5-fold). This is consistent with the observation of concentration profiles in Fig. 3. The value of $k_1$ for Sc(III) onto EDTA-functionalized magnetic silica was lower (i.e., 0.92 × $10^{-2}$ $min^{-1}$) than the value obtained with MPOH-MBA [91]. On the other hand, in this system, the PSORE gave a better fit of experimental profile. Similarly, Bao et al. [92] reported the better simulation of kinetic profiles with the PSORE for Sc(III) sorption onto a series of industrial resins (TP 260, TP 209, and TP 272) compared with PFORE: $k_2$ varied between 3.1 × $10^{-3}$ and 8.7 × $10^{-2}$ g $mmol^{-1}$ $min^{-1}$ (1.72–3.38 × $10^{-2}$ g $mmol^{-1}$ $min^{-1}$ for MPOH-MBA). The $k_1$ values were about one order of magnitude lower than for MPOH-MBA (in the range 0.92 × $10^{-2}$ – 3.45 × $10^{-3}$ $min^{-1}$).

Figure S8 confirms data reported in Table 1: the RIDE fails to correctly fit the profiles. However, it can be used for making a rough

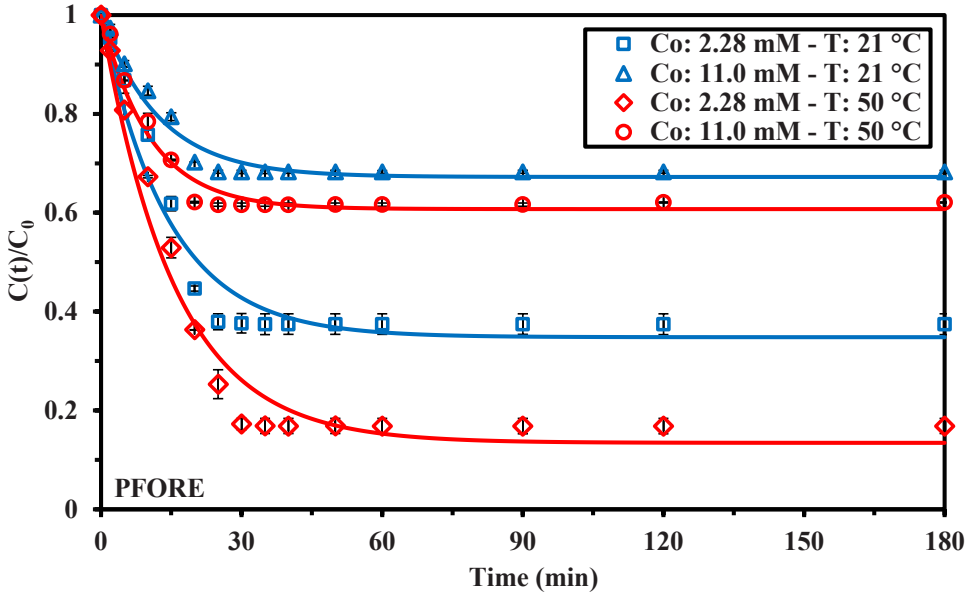


**Fig. 3.** Sc(III) uptake kinetics using MPOH-MBA for different initial concentrations and different temperatures – Modeling with the pseudo-first order rate equation ($pH_0$: 4.0; $C_0$: 2.28 or 11.0 mmol Sc $L^{-1}$; T: 21 ±1 °C or 50 ±1 °C; SD: 0.66 g $L^{-1}$; v- 210 rpm).

**Table 1**
Modeling of Sc(III) uptake kinetics using MPOH-MBA – Parameters of the models.

| | | | Temperature | | | |
|---|---|---|---|---|---|---|
| | | | 21 ±1 °C | | 50 ±1 °C | |
| Modeling | | | $C_0$ (mmol Sc $L^{-1}$) | | $C_0$ (mmol Sc $L^{-1}$) | |
| Model | Parameter | Unit | 2.28 | 11.0 | 2.28 | 11.0 |
| Experimental | $q_{eq,exp.}$ | mmol Sc $g^{-1}$ | 2.16 | 5.29 | 2.87 | 6.39 |
| PFORE | $q_{eq,1}$ | mmol Sc $g^{-1}$ | 2.25 | 5.46 | 2.99 | 6.54 |
| | $k_1 \times 10^2$ | $min^{-1}$ | 7.00 | 8.07 | 6.40 | 9.55 |
| | $R^2$ | | 0.966 | 0.975 | 0.978 | 0.982 |
| | AIC | | -88 | -114 | -87 | -114 |
| PSORE | $q_{eq,2}$ | mmol Sc $g^{-1}$ | 2.59 | 6.18 | 3.44 | 7.32 |
| | $k_2 \times 10^2$ | g $mmol^{-1}$ $min^{-1}$ | 3.38 | 1.72 | 2.31 | 1.79 |
| | $R^2$ | | 0.920 | 0.934 | 0.939 | 0.939 |
| | AIC | | -76 | -101 | -72 | -97 |
| RIDE | $D_e \times 10^{13}$ | $m^2$ $min^{-1}$ | 1.23 | 2.13 | 0.60 | 2.31 |
| | $R^2$ | | 0.927 | 0.951 | 0.937 | 0.957 |
| | AIC | | -76 | -104 | -69 | -101 |

evaluation of the order of magnitude of the effective diffusivity coefficient ($D_e$, $m^2$ $min^{-1}$): $D_e$ varies between $0.60 \times 10^{-13}$ $m^2$ $min^{-1}$ and $2.3 \times 10^{-13}$ $m^2$ $min^{-1}$; this is 5 orders of magnitude lower than the free diffusivity of Sc(III) in water (i.e., $3.44 \times 10^{-13}$ $m^2$ $min^{-1}$, [93]). This result confirms that the resistance to intraparticle diffusion cannot be neglected. The control of sorption kinetics involves contribution of the proper reaction rate (associated with the PFORE), the resistance to intraparticle diffusion (simulated by the RIDE), and probably other mechanism of resistance to diffusion (such as film diffusion to explain the failure of fits at contact time close to 15 min).

### 3.2.3. Sorption isotherms

The sorption isotherms (which represent the distribution of the solute at equilibrium between solid and liquid phase, for different concentrations) are compared under the same experimental conditions (i.e., at $pH_0$ 4, SD: 0.6 g $L^{-1}$) at two different temperatures (Fig. 4).

The curves are characterized by the progressive increase of the sorption capacity when the concentration increases up to $C_{eq}$: 4–6 mmol Sc $L^{-1}$, before stabilizing. The final plateau corresponds to the saturation of the sorbent. Consistently with the endothermic behavior already reported, both the saturation plateau and the initial slope of the curve (which is proportional to the Langmuir affinity coefficient) increase with the temperature. Hence, the maximum experimental sorption capacity increases from 5.34 to 6.50 mmol Sc $g^{-1}$ (from 21 °C to 50 °C).

Five models were tested for fitting sorption isotherms (see Table S1b). The statistical parameters ($R^2$ and AIC, in Table 2) clearly demonstrate that these models can be ranked according: Langmuir > Sips > Freundlich ≈ Dubinin-Radushkevich > Temkin. The Langmuir model (based on mechanistic approach) supposes that the sorption occurs as a monolayer with homogeneous distribution of sorption energies at the surface of the sorbent and without interaction between sorbed molecules. The empiric Freundlich equation assumes the sorption to be heterogeneous with possible interactions between sorbed molecules. The Sips equation introduces a supplementary third-adjustable parameter (by the combination of Langmuir and Freundlich equations). This model loses the physical dimension described in the Langmuir equation. Using three adjustable parameters is supposed improving the quality of mathematical fit; however, the calculation of the AIC (which considers the number of adjustable parameters) allows more accurate comparison of the quality of the fits. In Fig. 4, the sorption isotherms are plotted with superposition of Langmuir and Sips curves: these two panels show that the two models are highly qualitative in describing experimental profiles. The Langmuir model overestimates the maximum sorption capacity $q_{m,L}$ (by 22% at T: 21 °C and 10% at T: 50 °C), while the calculated $q_{m,S}$ values (for Sips equation) are even more overestimated (by 38% and 12%, respectively). The Langmuir affinity coefficient (i.e., $b_L$, L $mmol^{-1}$) is more than doubled when increasing the temperature: this is another proof of the endothermic character of Sc(III) sorption on MPOH-MBA.

Table S4 compares the Sc(III) sorption properties of a series of sorbents. The comparison of the different systems is made difficult by different experimental conditions (especially working pH). Solvent impregnated resins showed interesting application for acidic effluents [55,57] (at pH close to 1; despite slow kinetics limited by resistance to intraparticle diffusion, the weak sorption capacity is compensated by strong affinity coefficient). In intermediary acid regions (pH 2.5–3), extractant impregnated resin showed good sorption capacity ($q_{m,L}$: 1.71 mmol Sc $g^{-1}$, with good affinity, $b_L$: 45 L $mmol^{-1}$, and equilibrium reached in 720 min) [92]. TP 260 aminomethyl phosphonic resin exhibited fast sorption (≈90 min) with limited sorption capacity (about 0.244 mmol Sc $g^{-1}$) but remarkable affinity (i.e., 495 L $mmol^{-1}$). In the mild acid region (pH 4–5), some sorbents such as quaternized algal/PEI beads [86] and sulfonic-functionalized algal/PEI beads [40] reached excellent sorption capacities ($q_{m,L}$: 4.00–3.16 mmol Sc $g^{-1}$) with relatively fast process (40–90 min for equilibrium time) but low affinity coefficients ($b_L$: 1.26–0.56 L $mmol^{-1}$). However, MPOH-MBA demonstrates much higher global performances with sorption capacity as high as 6.5 mmol Sc $g^{-1}$, fast kinetics (≈30 min). This level of sorption is comparable to the capacity reached at pH 5.5 using $(NH_4)_2TiOF_4$ particles (i.e., up to 6 mmol Sc $L^{-1}$) [29]. The main drawback of MPOH-MBA concerns the weak affinity coefficient ($b_L$: 0.677 L $mmol^{-1}$). However, according to these first criteria, MPOH-MBA reveals a very promising sorbent for the removal of Sc(III) from mild acidic solutions.

### 3.2.4. Sorption mechanism

Considering the effect of pH (including optimal pH range, pH variation during sorption, and metal speciation), FTIR analysis (which showed the main contributions of carboxylate groups and phosphonate moieties in the binding of Sc(III), considered a hard acid). Tertiary amine groups (brought by iminodi(methylphosphonic acid) precursor) probably play a minor role in Sc(III) uptake due to steric hindrance effects. In addition, amine groups being considered intermediate base according "hard and soft acid and base" principles (HSAB, [94]) are expected to be less reactive for the binding of hard acids (such as Sc(III)), contrary to O-bearing ligands (such as carboxylate and phosphonate groups). The main reactivity of tertiary amine groups concerns, in acidic solution, the anion exchange of anionic scandium species on protonated reactive groups.

### 3.2.5. Selectivity

The selectivity of the sorbent for target metal is also a critical criterion for the treatment of real and complex effluents (which may contain a wide diversity of metals, whatever the source of effluent: leachate of

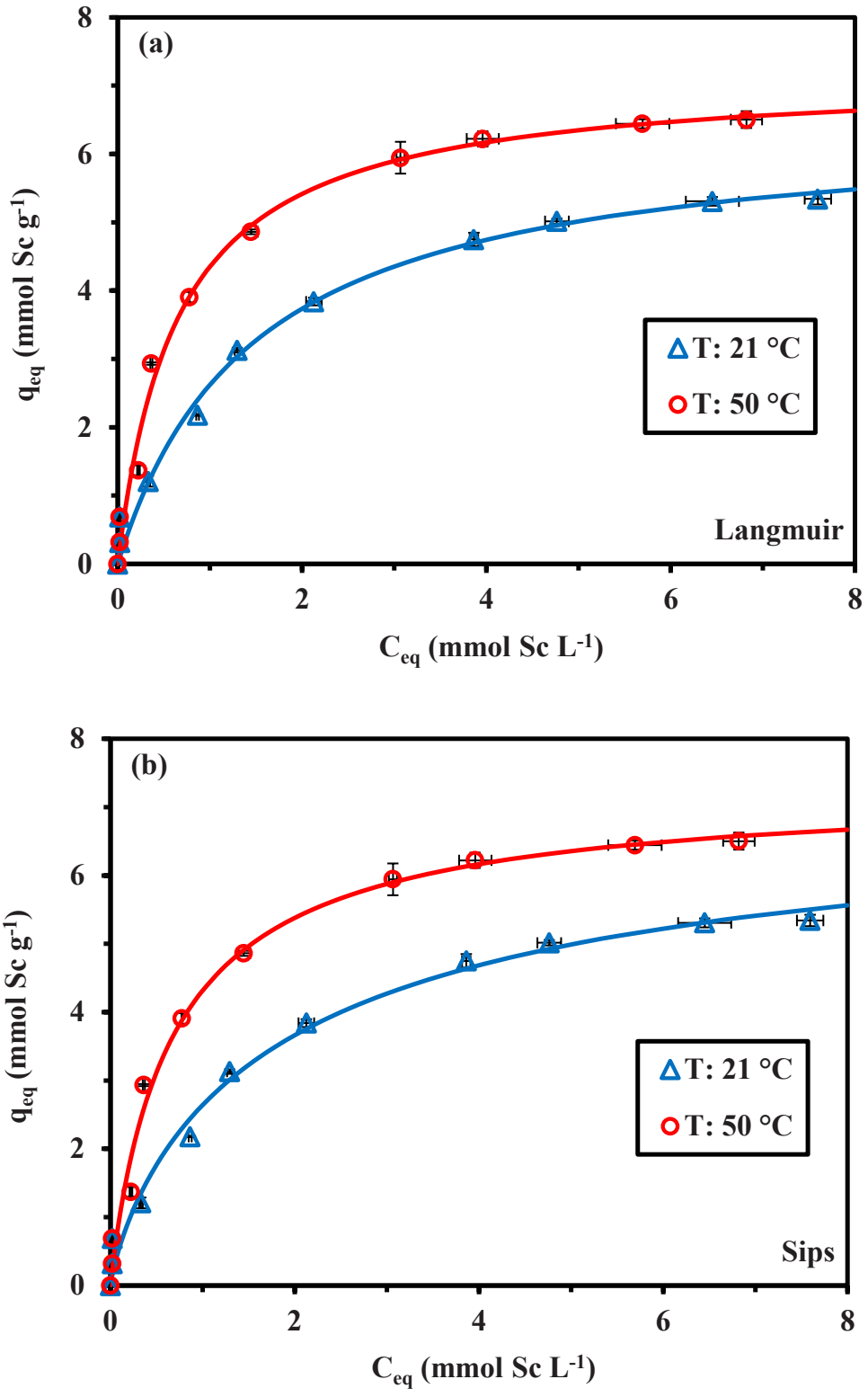


**Fig. 4.** Sc(III) sorption isotherms using MPOH-MBA for different temperatures – Modeling with the Langmuir (a) and Sips (b) equations ($pH_0$: 4.0; $C_0$: 0–11.0 mmol Sc $L^{-1}$; T: 21 ±1 °C or 50 ±1 °C; SD: 0.6 g $L^{-1}$; time: 48 h; v- 210 rpm).

ore or waste, mining residue, red mud). In order to evaluate the capacity of MPOH-MBA sorbent to recover Sc(III) from complex solution and optimize recovery processing, sorption tests are performed at different pH values using equimolar multi-metal solutions. For this purpose, selected competitor metals include alkali-earth metals (i.e., Ca(II) and Mg(II)), transition metals (Fe(III) and Zn(II)), post-transition metal from boron group (i.e. Al(III)), LREEs (i.e., light REE: La(III) and Ce(III)). It is noteworthy that Sc(III) is formally a transition metal but it is commonly considered a member of the REE family, and more specifically a HREE (heavy REE), based on its physicochemical characteristics (ionic size, etc., Table S5). Both divalent and trivalent cations are present at the same concentration (i.e., 1 ±0.1 mol $L^{-1}$). Figure S9 shows the

**Table 2**
Modeling of Sc(III) sorption isotherms using MPOH-MBA – Parameters of the models.

| Modeling | | | Temperature (°C) | |
|---|---|---|---|---|
| Model | Parameter | Unit | 21 ±1 | 50 ±1 |
| Experimental | $q_{m,exp.}$ | mmol Sc $g^{-1}$ | 5.34 | 6.50 |
| Langmuir | $q_{m,L}$ | mmol Sc $g^{-1}$ | 6.50 | 7.17 |
| | $b_L$ | L $mmol^{-1}$ | 0.677 | 1.54 |
| | $R^2$ | - | 0.993 | 0.992 |
| | AIC | - | -29 | -27 |
| Freundlich | $k_F$ | $mmol^{1-1/n_F}$ $L^{1/n_F}$ $g^{-1}$ | 2.59 | 3.73 |
| | n | - | 2.53 | 2.96 |
| | $R^2$ | - | 0.980 | 0.960 |
| | AIC | - | -22 | -9 |
| Sips | $q_{m,S}$ | mmol Sc $g^{-1}$ | 7.35 | 7.31 |
| | $b_S$ | $L^{1/n_S}$ $mmol^{-1/n_S}$ | 0.561 | 1.44 |
| | $n_S$ | - | 1.21 | 1.05 |
| | $R^2$ | - | 0.991 | 0.992 |
| | AIC | - | -26 | -23 |
| Temkin | $A_T$ | L $mmol^{-1}$ | 45.7 | 50.9 |
| | $b_T$ | J $kg^{-1}$ $mol^{-2}$ | 2860 | 2419 |
| | E | kJ $mol^{-1}$ | 0.535 | 0.372 |
| | $R^2$ | - | 0.921 | 0.962 |
| | AIC | - | -7 | -10 |
| D-R | $q_{D-R}$ | mmol $g^{-1}$ | 5.21 | 6.28 |
| | $b_{DR} \times 10^8$ | $mol^2$ $kJ^{-2}$ | 23.1 | 7.34 |
| | $E_{DR}$ | kJ $mol^{-1}$ | 2.079 | 3.69 |
| | $R^2$ | - | 0.976 | 0.983 |
| | AIC | - | -15 | -17 |

distribution of selected metals in the frame of covalent index ($CI = X_m^2 \times r$) *vs.* ionic index ($II = z^2 / r$) [95]. Most of these metals are classified as hard acids (or remain close to the frontier between hard acids (class A) and intermediate metals). According to the HSAB principles (Hard and Soft Acid and Base theory, [94]), hard acids prefer reacting with hard bases (meaning ligands bearing O-donor atoms, such as carboxylate and phosphonate, present in MPOH-MBA).

The comparison is performed through the selectivity coefficient ($SC_{Sc/metal}$, Fig. 5), the distribution ratio ($D_{metal}$, Figure S10), and the relative fraction of the different metals in the sorbent at equilibrium (Figure S11). The distribution ratios systematically increase with the pH of the solution (regardless of metal ion) (Figure S10). The ranking of the D values shows that MPOH-MBA has a marked preference for Sc(III) against:

$$La(III) > Ce(III) > Fe(III) > Al(III) \geq Mg(II) \geq Ca(II) \geq Zn(II) \quad (2)$$

At pH 4.91, the distribution ratio reaches 2.78 for Sc(III), while it drops to 1.08 for La(III) and 0.71 for Ce(III). This is qualitatively illustrated in Figure S9 by the increasing size of the distribution ratio: the largest bubbles correspond to trivalent cations, with a marked preference for REEs (D ranges between 0.71 for Ce(III) and up to 2.78 for Sc (III)); on the other hand, for divalent cations, D varies between 0.12 and 0.18 L $g^{-1}$. Giret el al. [49] compared different types of mesoporous silica for Sc(III) sorption in the presence of Al(III) and Fe(III), which were also significantly adsorbed (though the distribution ratios were significantly lower than for Sc(III)) and other REEs (with very low D values): the mesoporous silica particles are highly selective of Sc(III). In the case of TP 260 (aminomethyl phosphonic resin), the sorbent exhibited a significant selectivity coefficient for Sc(III) against Al(III) (up to 6) but moderate preference against Fe(III) ($SC_{Sc/Fe} \approx 1.32$) [92]. Much higher selectivity coefficients were reported against Fe(III) ($SC_{Sc/Fe} \approx 29.4$) and Al(III) ($SC_{Sc/Al} \approx 131$) with TP 272 (bis(2,4,4-trimethylpentyl) phosphinic acid resin). The change in the experimental conditions may affect the SC values; a direct comparison with other systems may be difficult. Herein, in Fig. 5a, the selectivity coefficient increases with the pH and according the sequence in Eq. 2. Notably, under optimum pH condition, the $SC_{Sc/metal}$ values range between 13 and 22 for Al(III) ≤ Mg(II) ≤ Ca(II) < Zn(II), meaning strong selectivity

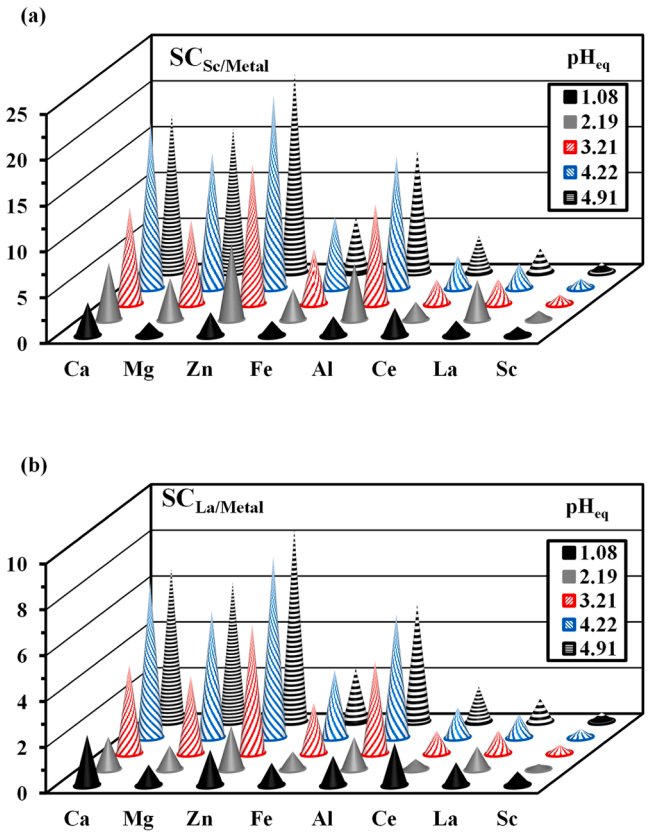


**Fig. 5.** Sc(III) (a) and La(III) (b) sorption from multi-component equimolar solutions – Selectivity coefficients *vs.* equilibrium pH ($C_0$: 1 mmol $L^{-1}$; SD: 1 g $L^{-1}$; time: 24 h; v- 210 rpm; $SC_{Sc/Sc} = 1$ and $SC_{La/La} = 1$, as relevant references).

against these metals. MPOH-MBA has lower separation properties against Fe(III) (≈6), Ce(III) (≈3.9), and La(III) (≈2.6). The ANOVA tests (not shown) on the effects of both the type of competitor metal and the pH on the $SC_{Sc/metal}$ show that the differences are statistically significant (at the 0.05 significance level for the F distribution, [48]). Fig. 5b offers an alternative vision of the selectivity issue: the selectivity coefficient $SC_{La/metal}$ is more than halved (compared with Sc selectivity).

The cumulative sorption capacity logically increases with pH (Table S6). At $pH_{eq}$ 4.22 (which corresponds to the working pH for the study of sorption isotherms), the cumulative sorption capacity reaches a value close to 2.37 mmol $g^{-1}$ ($C_{eq,Total}$: 5.98 mmol $L^{-1}$). For mono-component synthetic solution, the sorption isotherm shows a sorption capacity close to 5.2 mmol Sc $g^{-1}$ for the same residual concentration; this means that antagonist competition reduces the global sorption performance. The preference of MPOH-MBA for rare earths is clearly illustrated by Figure S11. While at $pH_{eq}$ 1.08, the sorption of Sc(III), La (III), and Ce(III) represent 43% (a little more than their relative fraction in the initial solution; i.e., 37.5%), when the pH exceeds 3, the REEs are concentrated in the sorbent: they represent about 67% of the total amount of bound metals.

Apparently, MPOH-MBA has a marked preference for trivalent metal ions against divalent metal ions. This result is consistent with the observations reported by Thapa et al. [96] in the case of bisphosphonate derivatives of $SiO_2$: the sorption were directly proportional to the ionic charge of co-existent metal ions. In addition, MPOH-MBA shows higher affinity for REEs (which have a tricapped trigonal prism configuration) against trivalent base metals (octahedral configuration). Despite their similar chemical properties (as Lewis acidity and atomic size), Thapa et al. [96] reported the higher selectivity for Sc(III) against trivalent cations ($Al^{3+}$ and $Fe^{3+}$); they correlated this behavior with lower

hydration enthalpy ($\Delta G_{hydr}$). Indeed, low $\Delta G_{hydr}$ values favor the dehydration step (prior to metal binding on sorption sites). In Table S5, $\Delta G_{hydr}$ varies between − 752 and − 907 kcal $mol^{-1}$ for studied REEs, while for trivalent cations, the value ranges between − 1019 and −1082 kcal $g^{-1}$. The small ionic size of Sc(III) (i.e., 0.87 Å, [97]) *vs.* La (III) and Ce(III) (1.216 and 1.196 Å) probably contributes to the higher selectivity of MPOH-MBA for scandium against other REEs; however, this preference may be also correlated with the differences in softness parameter (-0.52 *vs.* −0.75 and −0.72 for Sc(III), La(III) and Ce(III), respectively, [93]). Within REE's family, sorption is favored by small radius and high electronegativity (and high $pK_s$ and low $pK_a$): Sc >> La > Ce.

Among trivalent transition metals (not considering REEs), D increases with higher electronegativity and higher radius, higher covalent index ($X_m^2/r$) and lower ionic index ($z^2/r$): Fe > Al.

For divalent heavy metals, it was not possible establishing clear correlation between D and physicochemical criteria: Mg ≈ Ca > Zn. However, consistently with Thapa et al. [96], the distribution ratios are strictly lower for Mg(II), Ca(II), and Zn(II), because of the ionic charge.

### 3.3. Metal desorption and sorbent recycling

The effective evaluation of a new sorbent also requires characterizing (a) the capacity of the metal to be desorbed from loaded material, and (b) the possibility to re-use the sorbent for successive cycles. The sensitivity of metal sorption to pH gives a first orientation for the selection of desorption conditions: the binding of the metal may be reversed using acidic solutions. Zhao et al. [50] used sulfuric acid solution for eluting Sc(III) from aminocarbonylmethyl glycine: they showed that desorption efficiency increases with $H_2SO_4$ concentration (achieving total scandium release for 1 M concentration). This eluent was also very efficient for maintaining good stability at recycling. In the case of supported ionic liquid phase (SILP, on synthetic polymer support), Avdibegović et al. [45] compared the effect of acid concentration on the desorption of Sc(III): they also reported the good efficiency of sulfuric acid, and highlighted the necessity to use relatively concentrated solutions (i.e., 1 M). Sulfuric acid solution (2 M) was also used by Sharaf et al. [35] for eluting Sc(III) from binary-extractant (containing carboxylic acid and phosphonic-based organic phases) impregnated resin. Hamza et al. [40] used hydrochloric acid solution (0.2 M), completed with $CaCl_2$ (0.5 M) for Sc(III) release from sulfonic-functionalized algal/PEI beads (calcium chloride serving for the stabilization of algal compartment). In the study of Sc(III) separation from uranium leachates using Tulsion CH 93 (amino methyl phosphoric resin), Smirnov et al. [44] investigated alkaline and neutral solutions and found the best results for a mixture of $Na_2SO_4$ and $Na_2CO_3$. Artiushenko et al. [34] highlighted the interest of ligands for the elution of REEs from aminodiphosphonic acid-$SiO_2$ hybrids: ligands like EDTA require much lower concentrations than acidic solutions. Herein, desorption is processed with 0.3 M HCl solution. Figure S12 shows the kinetics of desorption for the different systems (T: 21/50 °C and $C_0$: 2.31/11.0 mmol Sc $L^{-1}$, for loading conditions). The kinetics profiles are very close, though the desorption efficiency is generally little better for the sorbents loaded with lower Sc(III) amounts. In any case, scandium is totally eluted in 15–20 min with $C_0$: 2.31 mmol Sc $L^{-1}$ samples, and 20–25 min for higher loading. Metal desorption is as fast as sorption.

Table 3 compares the sorption and desorption efficiencies for five successive cycles. It is noteworthy that scandium is totally desorbed at each step. On the other side, the stability in sorption efficiency (around 63% for selected experimental conditions) is remarkable: the loss between 1st and 5th cycle remains below 1.5%. This is consistent with the stability observed in FTIR spectra: the spectrum of the sorbent after being exposed to 5 cycles is very close to the spectrum of the pristine sorbent (Fig. 1, and Section 3.1.2.). These results demonstrate that MPOH-MBA has promising properties not only in terms of Sc(III) removal (kinetics and maximum sorption capacities) but also associated with remarkable stability. The concentration effect between sorption and desorption steps is limited to a factor 3 (considering the respective sorbent dose in the sorption and desorption steps; i.e., 0.66 g $L^{-1}$ and 2 g $L^{-1}$, respectively). This parameter would deserve complementary study to evaluate the optimum dose in the desorption step for achieving complete desorption with highest concentration effect.

**Table 3**
Sorbent recycling – Sorption and desorption efficiencies (SE and DE, %) for five successive cycles of sorption/desorption.

| Cycle | SE (%) | DE (%) |
|---|---|---|
| 1 | 63.9 ±0.6 | 100.1 ±0.0 |
| 2 | 63.7 ±0.5 | 100.2 ±0.0 |
| 3 | 63.4 ±0.7 | 99.9 ±0.0 |
| 4 | 63.3 ±0.7 | 100.2 ±0.5 |
| 5 | 63.0 ±0.7 | 100.2 ±0.3 |
| Loss at the 5th cycle | <1.5% | Negligible |

Experimental conditions – Sorption: C0, 2.31 mmol Sc L-1, SD, 0.660 g $L^{-1}$; pH0 4; time, 24 h; Desorption: 0.3 M HCl solution; SD, 2 g $L^{-1}$; time, 2 h; v, 210 rpm.

### 3.4. Application to red mud

#### 3.4.1. Effect of pH control – Precipitation issues

The red mud effluent (collected in the industrial site) is characterized by a very acidic pH ("negative" value). The composition of this raw effluent is reported in Table S2. The major elements are: Fe(III) (139 mmol Fe $L^{-1}$), Al(III) (16.4 mmol Al $L^{-1}$), and Si (1.11 mmol Si $L^{-1}$). Scandium represents up to 0.245 mmol Sc $L^{-1}$ (almost identical to Zn concentration), while traces of Ce(III), Zr(IV), and Mo(VI) are also detected (in the range 0.022–0.093 mmol $L^{-1}$).

A first treatment consisted in adjusting the pH to 1.01: the concentrations are hardly affected, as appearing in Table S2. The table also illustrates the large molar excess of major elements compared with Sc (III). Similar conclusion can be deduced at $pH_{eq}$ 2.99: molar excesses are of the same orders of magnitude (despite the precipitation effects, which represent metal losses between 9% and 20%). The precipitation dramatically increases when $pH_{eq}$ raises to 4.98. Most of iron precipitates (about 98%) with possible co-precipitation and/or entrapment of other metals including Al(III) (loss ≈80%), while the abatement of other metals varies between 42% and 54%, and up to 60% for Sc(III).

#### 3.4.2. Metal recovery from pre-treated effluents – Sorption onto MPOH-MBA

The sorption efficiencies are compared in Fig. 6. For trace metals, the sorption efficiencies reach up to 85% for Sc(III), 67% for Ce(III), 64% for Mo(VI), or 50% for Zr(IV), at $pH_{eq}$ 4.16. The sorption capacities for selected metal ions are reported in function of equilibrium pH in

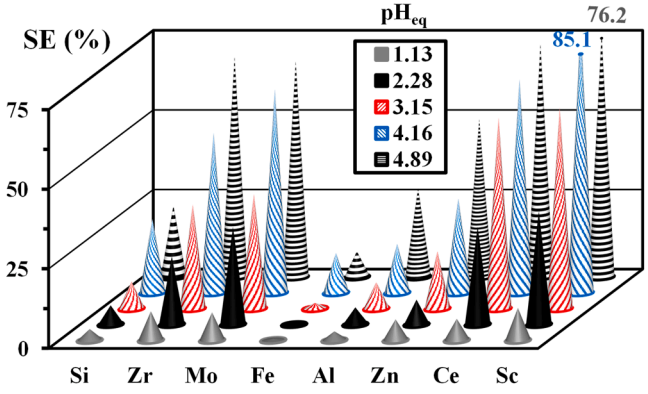


**Fig. 6.** Comparison of sorption efficiency (SE, %) for the different target metals from acid leachate of red mud in function of $pH_{eq}$ (SD: 1 g $L^{-1}$; time: 24 h; v-210 rpm; T: 21 ±1 °C).

Figure S13. The highest sorption capacities are obtained at $pH_{eq}$ 4.22; indeed, the strong precipitation occurring at higher pH reduces the efficiency of the process (due to the reduction of the effective metal concentration). The large excess of major elements (i.e., Fe(III) and Al (III)) naturally correlates with their high sorption capacities (Figure S13a). Figure S13b focuses on the sorption capacities of minor elements: sorption levels remain close to 0.12 mmol Sc $g^{-1}$, 0.17 mmol Si $g^{-1}$, and 0.045 mmol Zn $g^{-1}$ (other elements exhibit negligible uptake). The comparison of sorption performances may be carried out using other indicators such as sorption efficiency to modulate the effect of the large excess of major elements. The concentration factor (X-factor as the ratio between sorption capacity and initial metal concentration, Figure S14a) and the $SC_{Sc/metal}$ (Figure S14b) show complementary analysis of sorption and separation properties of MPOH-MBA in the treatment of acid leachate of red mud. Logically, the highest concentrating effects are obtained for minor elements: up to 5.7-folds for Sc (III). The enrichment is reduced for other minor elements not necessarily at the same $pH_{eq}$ (i.e., 4.16); indeed, for Mo(VI), Zr(IV), Zn(II), and Ce (III) it is necessary rising the $pH_{eq}$ to 4.89, but the X-factor remain below 3. The selectivity coefficient reflects in Figures S14b the correlation between huge excess of competitor metal and high $SC_{Sc/metal}$ values (this derives intrinsically from the SC formula). Obviously, these conditions do not allow reaching meaningful conclusions compared with experiments performed with equimolar concentrations (Section 3.2.5.). However, it may be interesting to observe that the highest $SC_{Sc/Fe}$ (i.e.; 92) is reached at $pH_{eq}$ 3.15, other elements are separated more efficiently at $pH_{eq}$ 4.16 with SC values reaching 31 for Al(III), 19 for Si(IV), 14 for Zn(II), and much lower values (below 6) for the other metals.

Meanwhile, the cumulative sorption capacities reach a maximum (close to 4 mmol $g^{-1}$) at $pH_{eq}$ 4.16. The cumulative sorption is directly influenced by the strong sorption of Fe(III) and Al(III), which represent between 85% and 93% of total sorption (depending on pH). This means that despite the relative preference of MPOH-MBA for Sc(III) (and other REEs), the presence of a huge excess of competitor transition metal ions strongly depreciates the efficiency of the sorbent for valuable critical metals. This limiting effect may be overexpressed by the impact of huge concentrations of counter anions. Making the best use of the outstanding qualities of MPOH-MBA would require pre-treating the effluent to modulate the huge excess of trivalent heavy cations.

The sorption properties of MPOH-MBA were compared with those of Q-APEI (algal/polyethyleneimine beads functionalized with quaternary amine groups, [86]) and S-$A_L$PEI (algal/polyethyleneimine beads functionalized with sulfonic acid groups, [40]). The same effluent (red mud leachate) was processed in the same experimental conditions. Figure S15 compares the $SC_{Sc/metal}$ values (at different equilibrium pH) for the three sorbents. The three sorbents show roughly similar trends: (a) higher selectivity coefficients against Fe(III) and Al(III) (major elements), (b) poor selectivity against Ce(III), Mo(VI), and Zr(IV). The sorbent having the lowest selectivity is Q-APEI (lower values of Sc coefficients); this is probably due to the predominance of weak base reactive groups. the loss is selectivity is mainly observed against Fe, Al, Zn and Si. S-$A_L$PEI sorbent shows an intermediary selectivity: the presence of sulfonic groups may explain the better separation properties of the sorbent compared with Q-APEI. Despite the slightly higher values of $SC_{Sc/Fe}$ for S-$A_L$PEI, MPOH-MPA globally shows better selectivity than S-based sorbent for the other metal ions. The diversity and density of O-donor ligands (especially phosphonate ligands) contributes to the preferential sorption of rare earth elements (Sc and Ce) than alternative materials. Figure S16 offers an alternative visualization of this comparison. The Figure individually compares MPOH-MBA with Q-APEI (Figure S16a) and with S-$A_L$PEI (Figure S16b) by the plot of SC values for MPOH-MBA vs. relevant values for the alternate sorbent ($SC_{Sc/Metal}$(MPOH-MBA)/ $SC_{Sc/Metal}$(sorbent)) at different pH values for the different metals (or metalloid). The comparison of the figures clearly shows that sorbents can be globally ranked according to: MPOH-MBA > S-$A_L$PEI >> Q-APEI. This ranking may be moderated by the pH value and the type of metal: Table S8 reports the optimum pH conditions for highest $SC_{SC/Metal}$ values for the three sorbents. MPOH-MBA allows reaching the highest separation of Sc from Si, Fe, Al, and Zn, while Q-APEI is slightly better for the separation of Sc from Zr and Ce, and S-$A_L$PEI reaches the highest selectivity against Mo. In any case, MPOH-MBA offers a good compromise while considering the complete series of metals (and metalloid), working at $pH_0$: 4.

The comparison of separation properties in the treatment of red mud leachates with data collected in the literature is made complex by the diversity in the composition of these solutions and/or the pre-treatment applied to these effluents. Table S7 summarizes some examples of results recently published in the treatment of red mud effluents. The results collected for MPOH-MBA are consistent with those referring to sorption systems. However, the best efficiency and selective separation performances were observed for systems involving dual treatments (i.e., solvent extraction and sorption). The complexity of the effluents and the huge excess of competitor trivalent metal cations (especially) requires combining complementary processes involving "positive" extraction (Sc recovery) and "negative" extraction (specific recovery of competitor ions). These results represent a first step in the design of a competitive process; at this stage they should be considered as a tool to complete the study of selective sorption (initiated on synthetic equimolar multicomponent solutions, at Section 3.2.5).

## 4. Conclusion

The valorization of secondary sources (such as red mud, low concentration effluents and leachates) is of critical importance for the recovery of valuable REEs, including scandium. One of the important challenges with this kind of effluent is the selective separation of valuable metals. The easy one-pot synthesis of MPOH-MBA reveals a promising method for producing of sorbent with outstanding sorption properties: (a) high sorption capacity (up to 5.34 mmol Sc $g^{-1}$) at mild acidic pH values (i.e., pH 4), (b) fast kinetics (equilibrium reached) in 20–30 min, (c) with good selectivity (compared to available literature), and (d) high capacity to be regenerated (with moderate acid solutions – 0.3 M HCl) and reused (negligible loss in sorption after 5 cycles). The coexistence of O-bearing groups (carboxylate and phosphonate) and N-bearing groups (tertiary amines) reveals favorable for reaching such remarkable properties. This new material opens promising perspectives compared with previous sorbents, as appearing in the comparison of sorption properties (including maximum sorption capacity, affinity coefficient or kinetic criteria), and selectivity issues. The investigation of selective sorption was investigated in a dual approach: (a) evaluation of selectivity issue at different pH values with equimolar multicomponent solutions, and (b) for the treatment of a real effluent (generated by the acidic leaching of red mud). MPOH-MBA shows a marked preference for trivalent cations including REEs, Fe(III) and Al(III) against divalent cations. Among trivalent cations, REEs are preferentially sorbed, and scandium (which is classified among the heavy REEs) is even preferred to Ce(III) and Nd(III)). This preference is correlated to the smaller ionic size of Sc(III) and its higher electronegativity. Applied to acidic leachate of red mud, MPOH-MBA allows recovery Sc(III) and Ce(III) with good efficiency (up to 80–85%) at moderate pH (i.e., $pH_{eq}$ 4.16). However, the huge excess of major elements (such as Fe and Al – 100- to 80-folds after precipitation at pH close to 5) limits the selectivity of the process. The valorization of the Sc(III) from this complex effluent will require combining different processes such as selective precipitation, and/or complementary solvent extraction process.

The outstanding Sc sorption properties of MPOH-MBA opens promising perspectives for the recovery of the metal in mild acidic conditions. However, these properties are based on batch investigations at small Lab-scale. The real promises should be evaluated at a larger scale in dynamic mode. This step in the evaluation of the sorbent requires experimenting fixed-bed columns or continuously stirred tank reactors. The small size of sorbent particles clearly favors the fast kinetics

reported in the study. However, this small size represents a critical drawback for application in fixed-bed columns (for head loss pressure and/or blockage) and agitated reactor at large scale (for solid/liquid separation). Obviously, the conditioning of the sorbent will be a necessary step for developing large scale application. There are different strategies that may be applied for facilitating the processing of these materials, including: (a) the incorporation of magnetite nanoparticles (for easy magnetic separation) [98], (b) the incorporation of porous material or deposition of the polymer on a porous sorbent [50], (c) the agglomeration of particles [50], (d) the shaping and spherization of the sorbent [99]. Obviously, the addition of charge into the sorbent (magnetic, porous support) presents some advantages but also some drawbacks (decrease in the volumetric density of reactive groups). The agglomeration of particles may also introduce some critical limitations to diffusion. Therefore, the shaping and conditioning of the material is a critical step in the final design of the sorbent as a compromise between high volumetric density of functional groups and availability and/or accessibility of reactive groups (for kinetic performance).

## Compliance with ethical standards

The Authors confirm that: (a) they do not have potential conflicts of interest, (b) research did not involve Human Participants and/or Animals.

The Authors confirm that they all read the submitted manuscript, and they all agreed the manuscript being submitted and, in case of acceptance, being published. They confirm their personal contributions (according the list cited above).


## Funding

This work was supported by the National Natural Science Foundation of China for supporting projects [U1967218, and 11975082] and by the National Key R&D Program of China (2022YFB3506100).


## CRediT authorship contribution statement

**Yuezhou Wei:** Conceptualization, Funding acquisition, Methodology. **Ji Wang:** Visualization, Investigation. **Xiangbiao Yin:** Validation, Data curation. **Shunyan Ning:** Visualization, Validation. **Hamed Mira:** Software, Formal analysis. **Mohammed F Hamza:** Writing – review & editing, Resources, Investigation, Conceptualization. **Eric Guibal:** Writing – review & editing, Writing – original draft, Conceptualization, Methodology, Software.

## Declaration of Competing Interest

The authors declare that they have no known competing financial interests or personal relationships that could have appeared to influence the work reported in this paper.

## Data Availability

Data will be made available on request.

## Appendix A. Supporting information

Supplementary data associated with this article can be found in the online version at doi:10.1016/j.colsurfa.2024.133875.

## References


[1] U.S. Geological Survey, in: Department of the Interior (Ed.), 2022 Final List of Critical Materials, Federal Register, Washington, DC, USA, 2022, pp. 10381–10382.

[2] D. Paderni, L. Giorgi, V. Fusi, M. Formica, G. Ambrosi, M. Micheloni, Chemical sensors for rare earth metal ions, Coord. Chem. Rev. 429 (2021) 213639, https://doi.org/10.1016/j.ccr.2020.213639.

[3] N. Dushyantha, N. Batapola, I.M.S.K. Ilankoon, S. Rohitha, R. Premasiri, B. Abeysinghe, N. Ratnayake, K. Dissanayake, The story of rare earth elements (REEs): Occurrences, global distribution, genesis, geology, mineralogy and global production, Ore Geol. Rev. 122 (2020) 103521, https://doi.org/10.1016/j.oregeorev.2020.103521.

[4] A. Yuksekdag, B. Kose-Mutlu, A.F. Siddiqui, M.R. Wiesner, I. Koyuncu, A holistic approach for the recovery of rare earth elements and scandium from secondary sources under a circular economy framework – A review, Chemosphere 293 (2022) 133620, https://doi.org/10.1016/j.chemosphere.2022.133620.

[5] Z. Liu, H. Li, Metallurgical process for valuable elements recovery from red mud-A review, Hydrometallurgy 155 (2015) 29–43, https://doi.org/10.1016/j.hydromet.2015.03.018.

[6] N. Zhang, H.-X. Li, X.-M. Liu, Recovery of scandium from bauxite residue-red mud: a review, Rare Met 35 (2016) 887–900, https://doi.org/10.1007/s12598-016-0805-5.

[7] S. Agrawal, N. Dhawan, Evaluation of red mud as a polymetallic source – A review, Miner. Eng. 171 (2021) 107084, https://doi.org/10.1016/j.mineng.2021.107084.

[8] M. Archambo, S.K. Kawatra, Red mud: Fundamentals and new avenues for utilization, Miner. Process. Extr. Metall. Rev. 42 (2021) 427–450, https://doi.org/10.1080/08827508.2020.1781109.

[9] A.B. Botelho Junior, D.C.R. Espinosa, J. Vaughan, J.A.S. Tenório, Recovery of scandium from various sources: a critical review of the state of the art and future prospects, Miner. Eng. 172 (2021) 107148, https://doi.org/10.1016/j.mineng.2021.107148.

[10] D. Zinoveev, L. Pasechnik, M. Fedotov, V. Dyubanov, P. Grudinsky, A. Alpatov, Extraction of valuable elements from red mud with a focus on using liquid media-A review, Recycling 6 (2021) 38, https://doi.org/10.3390/recycling6020038.

[11] A. Akcil, Y.A. Ibrahim, P. Meshram, S. Panda, Abhilash, Hydrometallurgical recycling strategies for recovery of rare earth elements from consumer electronic scraps: a review, J. Chem. Technol. Biotechnol. 96 (2021) 1785–1797, https://doi.org/10.1002/jctb.6739.

[12] H. Liu, H. Liu, C. Nie, J. Zhang, B.-M. Steenari, C. Ekberg, Comprehensive treatments of tungsten slags in China: a critical review, J. Environ. Manag. 270 (2020) 110927, https://doi.org/10.1016/j.jenvman.2020.110927.

[13] M. Mashkovtsev, M. Botalov, D. Smyshlyaev, R. Pajarre, P. Kangas, V. Rychkov, P. Koukkari, Pilot-scale recovery of rare earths and scandium from phosphogypsum and uranium leachates, in: P.B. Kowalczuk, J. Drzymala (Eds.), Mineral Engineering Conference MEC2016, Swieradow-Zdroj, Poland, 2016.

[14] A.A. Brouziotis, A. Giarra, G. Libralato, G. Pagano, M. Guida, M. Trifuoggi, Toxicity of rare earth elements: An overview on human health impact, Front. Environ. Sci. 10 (2022) 948041, https://doi.org/10.3389/fenvs.2022.948041.

[15] A. Ghosh, S. Dhiman, A. Gupta, R. Jain, Process evaluation of scandium production and its environmental impact, Environments 10 (2023) 8, https://doi.org/10.3390/environments10010008.

[16] Y. Chen, S. Ning, Y. Zhong, Z. Li, J. Wang, L. Chen, X. Yin, T. Fujita, Y. Wei, Study on highly efficient separation of zirconium from scandium with TODGA-modified macroporous silica-polymer based resin, Sep. Purif. Technol. 305 (2023) 122499, https://doi.org/10.1016/j.seppur.2022.122499.

[17] W. Zhang, S.Q. Yu, S.C. Zhang, J. Zhou, S.Y. Ning, X.P. Wang, Y.Z. Wei, Separation of scandium from the other rare earth elements with a novel macro-porous silica-polymer based adsorbent HDEHP/$SiO_2$-P, Hydrometallurgy 185 (2019) 117–124, https://doi.org/10.1016/j.hydromet.2019.01.012.

[18] W. Li, Z. Li, N. Wang, H. Gu, Selective extraction of rare earth elements from red mud using oxalic and sulfuric acids, J. Environ. Chem. Eng. 10 (2022) 108650, https://doi.org/10.1016/j.jece.2022.108650.

[19] P. Grudinsky, L. Pasechnik, A. Yurtaeva, V. Dyubanov, D. Zinoveev, Recovery of scandium, aluminum, titanium, and silicon from iron-depleted bauxite residue into valuable products: A case study, Crystals 12 (2022) 1578, https://doi.org/10.3390/cryst12111578.

[20] R. Kallio, U. Lassi, T. Kauppinen, E. Holappa, M. Christophliemk, S. Luukkanen, P. Tanskanen, T. Fabritius, Leaching characteristics of Sc-enriched, Fe-depleted acidic slags, Miner. Eng. 189 (2022) 107901, https://doi.org/10.1016/j.mineng.2022.107901.

[21] B. Yagmurlu, C. Dittrich, B. Friedrich, Effect of aqueous media on the recovery of scandium by selective precipitation, Metals 8 (2018) 314, https://doi.org/10.3390/met8050314.

[22] Q. Li, B. Ji, R. Honaker, A. Noble, W. Zhang, Partitioning behavior and mechanisms of rare earth elements during precipitation in acid mine drainage, Colloids Surf., A 641 (2022) 128563, https://doi.org/10.1016/j.colsurfa.2022.128563.

[23] T. Larochelle, A. Noble, K. Strickland, A. Ahn, P. Ziemkiewicz, J. Constant, D. Hoffman, C. Glascock, Recovery of rare earth element from acid mine drainage using organo-phosphorus extractants and ionic liquids, Minerals 12 (2022) 1337, https://doi.org/10.3390/min12111337.

[24] A. Merroune, J. Ait Brahim, B. Achiou, R. Boulif, E. Mahdi Mounir, R. Beniazza, Competitive extraction and stripping behaviors of rare earth elements from industrial wet-process phosphoric acid using di-(2-ethyl-hexyl) phosphoric acid solvent: Optimization and thermodynamic studies, J. Mol. Liq. 367 (2022) 120585, https://doi.org/10.1016/j.molliq.2022.120585.

[25] H. Pereira Neves, G. Max Dias Ferreira, G. Max Dias Ferreira, L. Rodrigues de Lemos, G. Dias Rodrigues, A.L. Versiane, A. Barbosa Mageste, Liquid-liquid extraction of rare earth elements using systems that are more environmentally friendly: Advances, challenges and perspectives, Sep. Purif. Technol. 282 (2022) 120064, https://doi.org/10.1016/j.seppur.2021.120064.

[26] D. Zou, Y.F. Deng, J. Chen, D.Q. Li, A review on solvent extraction of scandium, J. Rare Earths 40 (2022) 1499–1508, https://doi.org/10.1016/j.jre.2021.12.009.
[27] T.B. da Costa, M.G. Carlos da Silva, M.G. Adeodato Vieira, Biosorption of lanthanum using sericin/alginate/polyvinyl alcohol beads as a natural cation exchanger in a continuous fixed-bed column system, Colloids Surf., A 627 (2021) 127233, https://doi.org/10.1016/j.colsurfa.2021.127233.
[28] G.V. Briao, M.G. Carlos da Silva, M.G. Adeodato Vieira, Dysprosium adsorption on expanded vermiculite: Kinetics, selectivity and desorption, Colloids Surf., A 630 (2021) 127616, https://doi.org/10.1016/j.colsurfa.2021.127616.
[29] D. Sofronov, T. Blank, S. Khimchenko, A. Lebedynskiy, P. Mateychenko, V. Varchenko, M. Cherniakova, M. Rucki, W. Zurowski, Study on the sorption properties of $(NH_4)_2TiOF_4$ particles, Chem. Eng. J. 447 (2022) 137559, https://doi.org/10.1016/j.cej.2022.137559.
[30] M.G. Hamed, M.M.E. Breky, O. Ghazy, E.H. Borai, Separation and preconcentration of cerium (III) and Iron (III) on magnetic nanocomposite hydrogel, Colloids Surf., A 652 (2022) 129779, https://doi.org/10.1016/j.colsurfa.2022.129779.
[31] E. Ferizoglu, S. Kaya, Y.A. Topkaya, Solvent extraction behaviour of scandium from lateritic nickel-cobalt ores using different organic reagents, Physicochem. Probl. Miner. Process. 54 (2018) 538–545, https://doi.org/10.5277/ppmp1855.
[32] A.G.O. Souza, P. Aliprandini, D.C.R. Espinosa, J.A.S. Tenorio, Scandium extraction from nickel processing waste using Cyanex 923 in sulfuric medium, JOM 71 (2019) 2003–2009, https://doi.org/10.1007/s11837-019-03427-6.
[33] Z. Liu, H. Li, Q. Jing, M. Zhang, Recovery of scandium from leachate of sulfation-roasted bayer red mud by liquid-liquid extraction, JOM 69 (2017) 2373–2378, https://doi.org/10.1007/s11837-017-2518-0.
[34] O. Artiushenko, L. Kostenko, V. Zaitsev, Influence of competitive eluting agents on REEs recovery from silica gel adsorbent with immobilized aminodiphosphonic acid, J. Environ. Chem. Eng. 8 (2020) 103883, https://doi.org/10.1016/j.jece.2020.103883.
[35] M. Sharaf, W. Yoshida, F. Kubota, M. Goto, A novel binary-extractant-impregnated resin for selective recovery of scandium, J. Chem. Eng. Jpn. 52 (2019) 49–55, https://doi.org/10.1252/jcej.18we175.
[36] D.L. Ramasamy, S. Porada, M. Sillanpaa, Marine algae: A promising resource for the selective recovery of scandium and rare earth elements from aqueous systems, Chem. Eng. J. 371 (2019) 759–768, https://doi.org/10.1016/j.cej.2019.04.106.
[37] Y. Hosomomi, Y. Baba, F. Kubota, N. Kamiya, M. Goto, Biosorption of rare earth elements by *Escherichia coli*, J. Chem. Eng. Jpn. 46 (2013) 450–454, https://doi.org/10.1252/jcej.13we031.
[38] L. Zhang, C. Wang, R. Yang, G. Zhou, P. Yu, L. Sun, T. Hao, J. Wang, Y. Liu, Novel environment-friendly magnetic bentonite nanomaterials functionalized by carboxymethyl chitosan and 1-(2-pyridinylazo)-2-naphthaleno for adsorption of Sc (III), Appl. Surf. Sci. 566 (2021) 150644, https://doi.org/10.1016/j.apsusc.2021.150644.
[39] K. Komnitsas, D. Zaharaki, G. Bartzas, G. Alevizos, Adsorption of scandium and neodymium on biochar derived after low-temperature pyrolysis of sawdust, Minerals 7 (2017), https://doi.org/10.3390/min7100200.
[40] M.F. Hamza, K.A.M. Salih, A.A.H. Abdel-Rahman, Y.E. Zayed, Y. Wei, J. Liang, E. Guibal, Sulfonic-functionalized algal/PEI beads for scandium, cerium and holmium sorption from aqueous solutions (synthetic and industrial samples), Chem. Eng. J. 403 (2021) 126399, https://doi.org/10.1016/j.cej.2020.126399.
[41] X. Zhang, K. Zhou, Y. Wu, Q. Lei, C. Peng, W. Chen, Separation and recovery of iron and scandium from acid leaching solution of red mud using D201 resin, J. Rare Earths 38 (2020) 1322–1329, https://doi.org/10.1016/j.jre.2019.12.005.
[42] X. Zhu, W. Li, S. Tang, M. Zeng, P. Bai, L. Chen, Selective recovery of vanadium and scandium by ion exchange with D201 and solvent extraction using P507 from hydrochloric acid leaching solution of red mud, Chemosphere 175 (2017) 365–372, https://doi.org/10.1016/j.chemosphere.2017.02.083.
[43] K. Zhou, C. Teng, X. Zhang, C. Peng, W. Chen, Enhanced selective leaching of scandium from red mud, Hydrometallurgy 182 (2018) 57–63, https://doi.org/10.1016/j.hydromet.2018.10.011.
[44] A.L. Smirnov, S.M. Titova, V.N. Rychkov, G.M. Bunkov, V.S. Semenishchev, E. V. Kirillov, N.N. Poponin, I.A. Svirsky, Study of scandium and thorium sorption from uranium leach liquors, J. Radioanal. Nucl. Chem. 312 (2017) 277–283, https://doi.org/10.1007/s10967-017-5234-x.
[45] D. Avdibegovic, M. Regadio, K. Binnemans, Recovery of scandium(III) from diluted aqueous solutions by a supported ionic liquid phase (SILP), RSC Adv. 7 (2017) 49664–49674, https://doi.org/10.1039/c7ra07957e.
[46] D.L. Ramasamy, V. Puhakka, S. Iftekhar, A. Wojtus, E. Repo, S. Ben Hammouda, E. Iakovleva, M. Sillanpaa, N- and O- ligand doped mesoporous silica-chitosan hybrid beads for the efficient, sustainable and selective recovery of rare earth elements (REE) from acid mine drainage (AMD): Understanding the significance of physical modification and conditioning of the polymer, J. Hazard. Mater. 348 (2018) 84–91, https://doi.org/10.1016/j.jhazmat.2018.01.030.
[47] D.L. Ramasamy, V. Puhakka, E. Repo, S. Ben Hammouda, M. Sillanpaa, Two-stage selective recovery process of scandium from the group of rare earth elements in aqueous systems using activated carbon and silica composites: Dual applications by tailoring the ligand grafting approach, Chem. Eng. J. 341 (2018) 351–360, https://doi.org/10.1016/j.cej.2018.02.024.
[48] D.L. Ramasamy, V. Puhakka, E. Repo, M. Sillanpaa, Selective separation of scandium from iron, aluminium and gold rich wastewater using various amino and non-amino functionalized silica gels - A comparative study, J. Clean. Prod. 170 (2018) 890–901, https://doi.org/10.1016/j.jclepro.2017.09.199.
[49] S. Giret, Y. Hu, N. Masoumifard, J.-F. Boulanger, E. Juere, F. Kleitz, D. Lariviere, Selective separation and preconcentration of scandium with mesoporous silica, ACS Appl. Mater. Interfaces 10 (2018) 448–457, https://doi.org/10.1021/acsami.7b13336.
[50] Z.G. Zhao, Y. Baba, W. Yoshida, F. Kubota, M. Goto, Development of novel adsorbent bearing aminocarbonylmethylglycine and its application to scandium separation, J. Chem. Technol. Biotechnol. 91 (2016) 2779–2784, https://doi.org/10.1002/jctb.4884.
[51] J. Ma, Z. Wang, Y. Shi, Q. Li, Synthesis and characterization of lysine-modified SBA-15 and its selective adsorption of scandium from a solution of rare earth elements, RSC Adv. 4 (2014) 41597–41604, https://doi.org/10.1039/c4ra07571d.
[52] I.V. Burakova, A.B. Burakov, A.G. Tkachev, I.D. Troshkina, O.A. Veselova, A. V. Babkin, W.M. Aung, I. Ali, Kinetics of the adsorption of scandium and cerium ions in sulfuric acid solutions on a nanomodified activated carbon, J. Mol. Liq. 253 (2018) 277–283, https://doi.org/10.1016/j.molliq.2018,01.063.
[53] K. Kilian, K. Pyrzyńska, M. Pęgier, Comparative study of Sc(III) sorption onto carbon-based materials, Solvent Extr. Ion.-. Exch. 35 (2017) 450–459, https://doi.org/10.1080/07366299.2017.1354580.
[54] M. Pegier, K. Kilian, K. Pyrzynska, Enrichment of scandium by carbon nanotubes in the presence of calcium matrix, Microchem. J. 137 (2018) 371–375, https://doi.org/10.1016/j.microc.2017.11.012.
[55] J.-Y. Moon, C. Takajo, S. Nishihama, K. Yoshizuka, Separation and recovery of scandium and yttrium from aqueous chloride media by integrated ion exchange method, Solvent Extr. Res. Dev., Jpn. 27 (2020) 91–97, https://doi.org/10.15261/serdj.27.91.
[56] Q. Yu, S. Ning, W. Zhang, X. Wang, Y. Wei, Recovery of scandium from sulfuric acid solution with a macro porous TRPO/$SiO_2$-P adsorbent, Hydrometallurgy 181 (2018) 74–81, https://doi.org/10.1016/j.hydromet.2018.07.025.
[57] H.M. Cui, J. Chen, H.L. Li, D. Zou, Y. Liu, Y.F. Deng, High-performance polymer-supported extractants with phosphonate ligands for scandium(III) separation, AlChE J. 62 (2016) 2479–2489, https://doi.org/10.1002/aic.15236.
[58] Y.M. Polikarpov, F.I. Belskii, S.V. Matveev, T.Y. Medved, M.I. Kabachnik, Synthesis and study of complexing properties of xylylenediaminotetra(methylphosphonic) acids, Bull. Acad. Sci. USSR - Div. Chem. Sci. 31 (1982) 635–637, https://doi.org/10.1007/bf00949804.
[59] E.G. Afonin, Iminodi(methylphosphonic) acid, Russ. J. Gen. Chem. 73 (2003) 1503–1505, https://doi.org/10.1023/B:RUGC.0000016010.34401.4f.
[60] S. Yamakawa, K. Oshita, A. Sabarudin, M. Oshima, S. Motomizu, Synthesis of iminodi(methylphosphonic acid)-type chitosan resin and its adsorption behavior for trace metals, Bunseki Kagaku 53 (2004) 1039–1043, https://doi.org/10.2116/bunsekikagaku.53.1039.
[61] L. Biro, B. Toth, N. Lihi, E. Farkas, P. Buglyo, Interaction between $[(\eta_6\text{-p-cym})M(H_2O)_3]^{2+}$ ($M^{II}$ = Ru, Os) or $(\eta^5\text{-Cp}^*)M(H_2O)_3]^{2+}$ ($M^{III}$ = Rh, Ir) and phosphonate derivatives of iminodiacetic acid: A solution equilibrium and DFT study, Molecules 28 (2023) 1477, https://doi.org/10.3390/molecules28031477.
[62] L. Cunha-Silva, S. Lima, D. Ananias, P. Silva, L. Mafra, L.D. Carlos, M. Pillinger, A. A. Valente, F.A. Almeida Paz, J. Rocha, Multi-functional rare-earth hybrid layered networks: photoluminescence and catalysis studies, J. Mater. Chem. 19 (2009) 2618–2632, https://doi.org/10.1039/b817381h.
[63] L. Cunha-Silva, D. Ananias, L.D. Carlos, F.A. Almeida Paz, J. Rocha, Synchrotron powder structure of a new layered lanthanide-organic network, Z. Krist. 224 (2009) 261–272, https://doi.org/10.1524/zkri.2009.1132.
[64] G.A. Pereira, J.A. Peters, F.A.A. Paz, J. Rocha, C. Geraldes, Evaluation of Ln $(H_2cmp)(H_2O)$ metal organic framework materials for potential application as magnetic resonance imaging contrast agents, Inorg. Chem. 49 (2010) 2969–2974, https://doi.org/10.1021/ic9025014.
[65] M. Cao, S. Sun, C. Long, J. Luo, D. Wu, Microporous metal phosphonate-based N-doped graphene oxide for efficient electrocatalyst for water oxidation, Mater. Lett. 284 (2021) 128891, https://doi.org/10.1016/j.matlet.2020.128891.
[66] P. Bhanja, Y. Kim, K. Kani, B. Paul, T. Debnath, J. Lin, A. Bhaumik, Y. Yamauchi, Novel porous metal phosphonates as efficient electrocatalysts for the oxygen evolution reaction, Chem. Eng. J. 396 (2020) 125245, https://doi.org/10.1016/j.cej.2020.125245.
[67] P. Bhanja, B. Mohanty, B. Paul, A. Bhaumik, B.K. Jena, S. Basu, Novel microporous organic-inorganic hybrid metal phosphonates as electrocatalysts towards water oxidation reaction, Electrochim. Acta 416 (2022) 140277, https://doi.org/10.1016/j.electacta.2022.140277.
[68] P. Bhanja, T. Dam, S. Chatterjee, A. Bhaumik, A. Ghosh, Lithium embedded hierarchically porous aluminium phosphonate as anode material for lithium-polymer battery, Mater. Sci. Eng., B 274 (2021) 115490, https://doi.org/10.1016/j.mseb.2021.115490.
[69] K.A.M. Salih, K. Zhou, M.F. Hamza, H. Mira, Y. Wei, S. Ning, E. Guibal, W. M. Salem, Phosphonation of alginate-polyethyleneimine beads for the enhanced removal of Cs(I) and Sr(II) from aqueous solutions, Gels 9 (2023) 152, https://doi.org/10.3390/gels9020152.
[70] Y.C. You, J.L. Jiao, Z. Li, C.Y. Zhu, Synthesis and swelling behavior of crosslinked copolymers of neutralized maleic anhydride with other monomers, J. Appl. Polym. Sci. 88 (2003) 2725–2731, https://doi.org/10.1002/app.11804.
[71] Y. Zhou, Q. Jin, X. Hu, Q. Zhang, T. Ma, Heavy metal ions and organic dyes removal from water by cellulose modified with maleic anhydride, J. Mater. Sci. 47 (2012) 5019–5029, https://doi.org/10.1007/s10853-012-6378-2.
[72] W. Gui, Y. Yang, X. Zhu, High-efficiency recovery of rare earth ions by hydrolyzed poly(styrene-co-maleic anhydride), J. Appl. Polym. Sci. 133 (2016) 43676, https://doi.org/10.1002/app.43676.
[73] F.N. Bahmanova, Thorium(IV) preconcentration by chelate-forming adsorbents based on a maleic anhydride-styrene copolymer, J. Anal. Chem. 75 (2020) 1116–1119, https://doi.org/10.1134/s106193482009004x.
[74] S. Simsek, E. Yilmaz, A. Boztug, Amine-modified maleic anhydride containing terpolymers for the adsorption of uranyl ion in aqueous solutions, J. Radioanal. Nucl. Chem. 298 (2013) 923–930, https://doi.org/10.1007/s10967-013-2529-4.

[75] R. Hasanzadeh, P.N. Moghadam, N. Bahri-Laleh, E.N. Zare, Sulfonated magnetic nanocomposite based on reactive PGMA-MAn copolymer@$Fe_3O_4$ nanoparticles: Effective removal of Cu(II) ions from aqueous solutions, Int. J. Polym. Sci. 2016 (2016) 2610541, https://doi.org/10.1155/2016/2610541.
[76] M. Szkudlarek, E. Heine, H. Keul, U. Beginn, M. Moller, Synthesis, characterization, and antimicrobial properties of peptides mimicking copolymers of maleic anhydride and 4-methyl-1-pentene, Int. J. Mol. Sci. 19 (2018) 2617, https://doi.org/10.3390/ijms19092617.
[77] N. Ni, D.H. Zhang, M.J. Dumont, Synthesis and characterization of zein-based superabsorbent hydrogels and their potential as heavy metal ion chelators, Polym. Bull. 75 (2018) 31–45, https://doi.org/10.1007/s00289-017-2017-z.
[78] S.F. M. Yusoff, F. Firdaus, N.A.A. Zahidi, N.H.A. Halim, Optimization, kinetics isotherm, and reusability studies of methylene blue dye adsorption using acrylic acid grafted rubber hydrogel, Sains Malays. 51 (2022) 3307–3320, https://doi.org/10.17576/jsm-2022-5110-16.
[79] J. Piatek, C.N. de Bruin-Dickason, A. Jaworski, J.H. Chen, T. Budnyak, A. Slabon, Glycine-functionalized silica as sorbent for cobalt(II) and nickel(II) recovery, Appl. Surf. Sci. 530 (2020) 147299, https://doi.org/10.1016/j.apsusc.2020.147299.
[80] O. Falyouna, O. Eljamal, I. Maamoun, A. Tahara, Y. Sugihara, Magnetic zeolite synthesis for efficient removal of cesium in a lab-scale continuous treatment system, J. Colloid Interface Sci. 571 (2020) 66–79, https://doi.org/10.1016/j.jcis.2020.03.028.
[81] M. Thommes, K. Kaneko, A.V. Neimark, J.P. Olivier, F. Rodriguez-Reinoso, J. Rouquerol, K.S.W. Sing, Physisorption of gases, with special reference to the evaluation of surface area and pore size distribution (IUPAC Technical Report), Pure Appl. Chem. 87 (2015) 1051–1069, https://doi.org/10.1515/pac-2014-1117.
[82] D. Lin-Vien, N.B. Colthup, W.G. Fateley, J.G. Grasselli, CHAPTER 16 - Organophosphorus Compounds, in: D. Lin-Vien, N.B. Colthup, W.G. Fateley, J. G. Grasselli (Eds.), The Handbook of Infrared and Raman Characteristic Frequencies of Organic Molecules, Academic Press, San Diego, 1991, pp. 263–276.
[83] D. Lin-Vien, N.B. Colthup, W.G. Fateley, J.G. Grasselli, CHAPTER 9 - Compounds Containing the Carbonyl Group, in: D. Lin-Vien, N.B. Colthup, W.G. Fateley, J. G. Grasselli (Eds.), The Handbook of Infrared and Raman Characteristic Frequencies of Organic Molecules, Academic Press, San Diego, 1991, pp. 117–154.
[84] G.B. Deacon, R.J. Phillips, Relationships between the carbon-oxygen frequencies of carboxylato complexes and the type of carboxylate coordination, Coord. Chem. Rev. 33 (1980) 227–250, https://doi.org/10.1016/s0010-8545(00)80455-5.
[85] J. Coates, Interpretation of Infrared Spectra, A Practical Approach, in: R.A. Meyers (Ed.), Encyclopedia of Analytical Chemistry, John Wiley & Sons Ltd, Chichester, U. K., 2000, pp. 10815–10837.
[86] M.F. Hamza, Y. Wei, E. Guibal, Quaternization of algal/PEI beads (a new sorbent): characterization and application to scandium recovery from aqueous solutions, Chem. Eng. J. 383 (2020) 123210, https://doi.org/10.1016/j.cej.2019.123210.
[87] A.A. Galhoum, Facile synthesis of functionalized polyglycidyl methacrylate-magnetic nanocomposites for enhanced uranium sorption, RSC Adv. 9 (2019) 38783–38796, https://doi.org/10.1039/c9ra06874k.
[88] X. Teng, Y. Niu, Z. Xie, Q. Cai, Synthesis and application of acrylamide-maleic anhydride copolymer for solid phase extraction, IOP Conf. Ser.: Mater. Sci. Eng. 322 (2018) 022013, https://doi.org/10.1088/1757-899X/322/2/022013.
[89] A. Gurjar, P. Sinha, R.K. Bansal, Tandem Michael addition of amines to maleic anhydride and 1,3-prototropic shift: experimental and theoretical results, Tetrahedron 70 (2014) 5052–5056, https://doi.org/10.1016/j.tet.2014.06.003.
[90] C. Wang, L. Zhang, G. Zhou, J. Qiu, Y. Liu, R. Yang, J. Chi, J. Wang, Synthesis of environmental-friendly ion-imprinted magnetic nanocomposite bentonite for selective recovery of aqueous Sc(III), J. Colloid Interface Sci. 630 (2023) 738–750, https://doi.org/10.1016/j.jcis.2022.10.161.
[91] A.D. Salman, T. Juzsakova, R. Akos, R.I. Ibrahim, M.A. Al-Mayyahi, S. Mohsen, T. A. Abdullah, E. Domokos, Synthesis and surface modification of magnetic $Fe_3O_4$@$SiO_2$ core-shell nanoparticles and its application in uptake of scandium (III) ions from aqueous media, Environ. Sci. Pollut. Res. 28 (2021) 28428–28443, https://doi.org/10.1007/s11356-020-12170-4.
[92] S. Bao, W. Hawker, J. Vaughan, Scandium loading on chelating and solvent impregnated resin from sulfate solution, Solvent Extr. Ion.-. Exch. 36 (2018) 100–113, https://doi.org/10.1080/07366299.2017.1412917.
[93] Y. Marcus, Ion Properties, Marcel Dekker, Inc, New York, NY, 1997.
[94] R.G. Pearson, Acids and bases, Sci. (N. Y., N. Y. ) 151 (1966) 172–177, https://doi.org/10.1126/science.151.3707.172.
[95] E. Nieboer, D.H.S. Richardson, The replacement of the non-descript term 'heavy-metals' by a biologically and chemically significant classification of metal-ions, Environ. Pollut. Ser. B 1 (1980) 3–26, https://doi.org/10.1016/0143-148x(80)90017-8.
[96] R. Thapa, T. Nissinen, P. Turhanen, J. Määttä, J. Vepsäläinen, V.-P. Lehto, J. Riikonen, Bisphosphonate modified mesoporous silicon for scandium adsorption, Microporous Mesoporous Mater. 296 (2020) 109980, https://doi.org/10.1016/j.micromeso.2019.109980.
[97] I. Persson, Hydrated metal ions in aqueous solution: How regular are their structures? Pure Appl. Chem. 82 (2010) 1901–1917, https://doi.org/10.1351/pac-con-09-10-22.
[98] L. Kostenko, N. Kobylinska, S. Khainakov, S.G. Granda, Magnetite nanoparticles with aminomethylenephosphonic groups: synthesis, characterization and uptake of europium(III) ions from aqueous media, Microchim. Acta 186 (2019) 474, https://doi.org/10.1007/s00604-019-3520-8.
[99] A. Abramova, N. Couzon, M. Leloire, P. Nerisson, L. Cantrel, S. Royer, T. Loiseau, C. Volkringer, J. Dhainaut, Extrusion-spheronization of UiO-66 and UiO-66_$NH_2$ into robust-shaped solids and their use for gaseous molecular iodine, xenon, and krypton adsorption, ACS Appl. Mater. Interfaces 14 (2022) 10669–10680, https://doi.org/10.1021/acsami.1c21380.